

UMOEA/D: A Multiobjective Evolutionary Algorithm for Uniform Pareto Objectives based on Decomposition

Xiaoyuan Zhang¹ Xi Lin¹ Yichi Zhang² Yifan Chen³ Qingfu Zhang¹

Abstract

Multiobjective optimization (MOO) is prevalent in numerous applications, in which a Pareto front (PF) is constructed to display optima under various preferences. Previous methods commonly utilize the set of Pareto objectives (particles on the PF) to represent the entire PF. However, the empirical distribution of the Pareto objectives on the PF is rarely studied, which implicitly impedes the generation of diverse and representative Pareto objectives in previous methods. To bridge the gap, we suggest in this paper constructing *uniformly distributed* Pareto objectives on the PF, so as to alleviate the limited diversity found in previous MOO approaches. We are the first to formally define the concept of “uniformity” for an MOO problem. We optimize the maximal minimal distances on the Pareto front using a neural network, resulting in both asymptotically and non-asymptotically uniform Pareto objectives. Our proposed method is validated through experiments on real-world and synthetic problems, which demonstrates the efficacy in generating high-quality uniform Pareto objectives and the encouraging performance exceeding existing state-of-the-art methods. The detailed model implementation and the code are scheduled to be open-sourced upon publication.

1. Introduction

Real-world applications such as trustworthy machine learning (Zhao & Gordon, 2022; Liang et al., 2021), autonomous agent planning (Xu et al., 2020; Hayes et al., 2022), and industrial design (Schulz et al., 2017; Wang et al., 2011; Tanabe & Ishibuchi, 2020; Xu et al., 2021) often involve multiobjective optimization (MOO) problems. The most important insight from MOO is that due to the conflicting

¹Department of Computer Science, City University of Hong Kong ²Department of Biostatistics and Bioinformatics, Duke University ³Departments of Computer Science and Mathematics, Hong Kong Baptist University.

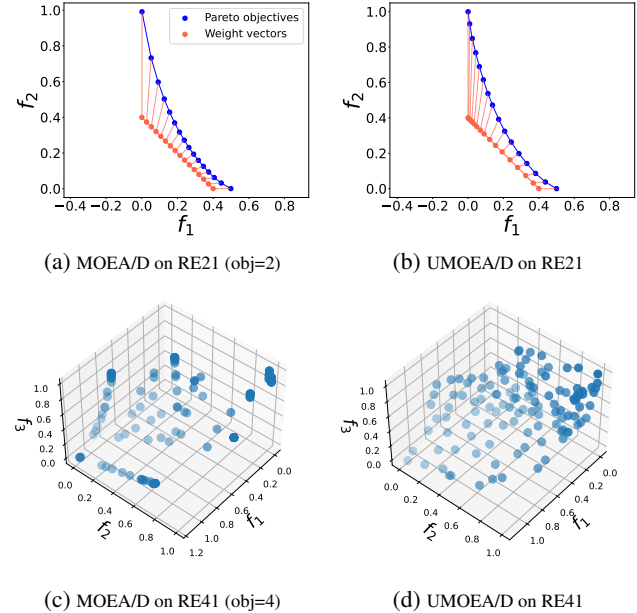


Figure 1. (a)/(c): MOEA/D produces non-uniform and potentially duplicated solutions. (b)/(d): UMOEA/D generates uniform objectives on the PF by searching for a set of weight vectors. RE41 is a 4-objective problem, and its objective space is projected onto the first three objectives for visualization.

nature between different objectives, simultaneously achieving optima for all objectives is difficult. For example, for a fairness classification system, it is essential for a decision maker to balance a trade-off between conflicting objectives, e.g., accuracy and fairness, to make a trustworthy decision (Zhao & Gordon, 2022; Ruchte & Grabocka, 2021; Xian et al., 2023).

The concept of Pareto optimality is thereby introduced to resolve such conflict. A solution \mathbf{x} is called Pareto optimal if it cannot be dominated by any other solution \mathbf{x}' in the decision space: more specifically, we will have if $f_i(\mathbf{x}) \leq f_i(\mathbf{x}')$, for some $i \in [m]$, then there must exist $j \in [m]$ such that $f_j(\mathbf{x}) > f_j(\mathbf{x}')$; Here $\mathbf{f}(\mathbf{x})$ is an m -objective vector function and $[m] = \{1, \dots, m\}$ (Miettinen, 1999; Ehrgott, 2005). An illustrative example of Pareto objectives for a two-objective problem can be seen in Figure 1(a) or (b),

where one objective (e.g. f_1) cannot be decreased without deteriorating the other objective (e.g. f_2). The collection of all Pareto solutions is dubbed as the Pareto set (PS), and its corresponding objectives form the PF.

In the past few decades, a large amount of MOO algorithms (Zhang & Li, 2007; Zhang et al., 2008; Li et al., 2014; Lin et al., 2019; Liu et al., 2021b; Bernreuther et al., 2023) have been proposed for constructing a finite set of solutions (termed as a ‘‘population’’ in MOO) to approximate the PF. Among them, multiobjective evolutionary algorithms (MOEAs) are the most popular due to their capability to avoid poor local optima and obtain a set of solutions in a single run (Blank & Deb, 2020; Caramia et al., 2020).

1.1. Challenges for constructing uniform PF

One pursuit for contemporary MOEAs research is to efficiently generate Pareto objectives *uniformly* distributed on the PF; which are considered effectively capturing the entire PF since they represent diverse optimal trade-offs among multiple objectives.

To achieve that, a flurry of efforts have been made to generate uniform weight vectors (Blank et al., 2020; Liu et al., 2021a; Das & Dennis, 1998; Elarbi et al., 2019) aiming to approximate uniform Pareto objectives consequently. However, it has been noted in recent work (Rhee et al., 2017; Liu et al., 2021b), that uniform weights do not necessarily yield uniform objectives. Illustrative examples are shown in Figure 1, where Figures 1(a) and (c) on the left reflect MOEA/D (multiobjective evolutionary algorithm based on decomposition) (Zhang & Li, 2007) adopts uniform weight vectors but obtains non-uniform and possibly duplicate Pareto objectives. (In contrast, our method, as shown in Figures 1(b) and (d), manages to generate uniform Pareto objectives for both a two-objective and a four-objective problem.)

A straightforward way to address the issue of non-uniform Pareto objectives is to search for a set of weight factors that corresponding to uniform Pareto objectives. The first notable work in this line is MOEA/D-AWA (Qi et al., 2014, MOEA with adaptive weight adjustment by decomposition). Subsequently, numerous follow-up works developed similar weight adjustment algorithms (de Farias et al., 2018; Siwei et al., 2011; Wu et al., 2017; Dong et al., 2020; Jiao et al., 2021). In general, these methods employ simple models to estimate the underlying PF (Wu et al., 2017; Dong et al., 2020) and use heuristic strategies to adjust weights, such as removing the most crowded solutions and adding the most sparse ones (de Farias et al., 2018). However, those methods perform poorly in certain scenarios due to the reliance on heuristic strategies.

1.2. Our contributions

In this paper, we propose UMOEA/D, the first principled method to generate Uniform Pareto objectives under the MOEA/D (D denotes decomposition) framework (Zhang & Li, 2007). We propose formal definitions of ‘‘uniformity’’ on the PF. We demonstrate that maximizing the minimal pairwise distances in a finite set yields both asymptotic and non-asymptotic uniformity guarantees. To numerically strengthen the search process, we employ a neural network to approximate the shape of the PF. The empirical results show that our method can generate high-quality uniform Pareto objectives in a reasonable time for both synthetic and real-world industrial design problems with a large number of locally optimal solutions. Those problems are challenging to gradient-based MOO methods (Mahapatra & Rajan, 2020; Liu et al., 2021b). UMOEA/D outperforms state-of-the-art methods in terms of both solution quality and running time.

In summary, the contribution of this paper is three-fold.

1. We study the deficiency of MOEA/D in achieving uniform Pareto objectives, which rooted in the non-linearity of the ‘‘weight-to-objective’’ function $h(\cdot)$ and investigate the characteristics of this function.
2. We propose UMOEA/D, an NN-based scheme to obtain uniform Pareto objectives by modeling $h(\cdot)$ to minimize a rigorously defined uniformity score, along with provable asymptotic and non-asymptotic results.
3. We conducted extensive experiments on both synthetic and real-world MOO problems. Results demonstrate that UMOEA/D outperforms state-of-the-art methods in terms of both the uniformity of solutions and runtime efficiency.

2. Multiobjective preliminaries

In this section, we provide a concise overview of key concepts in MOO. For clarity, throughout this paper, bold lower letters denote vectors (e.g. \boldsymbol{v}), bold upper letters denote a set of vectors (e.g., \boldsymbol{Y}). A multiobjective problem (MOP) of m conflicting objectives can be expressed as:

$$\min_{\boldsymbol{x} \in \mathcal{X} \subset \mathbb{R}^n} \boldsymbol{f}(\boldsymbol{x}) = (f_1(\boldsymbol{x}), \dots, f_m(\boldsymbol{x})), \quad (1)$$

where the min operator is formally reloaded and different from the minimization operator in the scalar case.

Notably, for an MOO problem, it is difficult to compare two solutions and the concepts of domination and Pareto optimal solutions are thereby introduced. We say a solution $\boldsymbol{x}^{(a)}$ **dominates** $\boldsymbol{x}^{(b)}$ if there exists an index $i \in [m]$ such that $f_i(\boldsymbol{x}^{(a)}) < f_i(\boldsymbol{x}^{(b)})$ and $\forall j \in [m] \setminus \{i\}, f_j(\boldsymbol{x}^{(a)}) \leq f_j(\boldsymbol{x}^{(b)})$. A solution \boldsymbol{x} is a **Pareto solution** if no other solution $\boldsymbol{x}' \in \mathcal{X}$ dominates it. The set of all Pareto solutions is denoted as the **Pareto set** PS, and its image set \mathcal{T} , $\mathcal{T} = (f \circ \text{PS})$ is called the **Pareto front** (PF). The

dominance of a solution $\mathbf{x}^{(a)}$ over another solution $\mathbf{x}^{(b)}$ implies that $\mathbf{x}^{(a)}$ is strictly better than $\mathbf{x}^{(b)}$, which indicates that $\mathbf{x}^{(b)}$ can be dropped in MOO. For a Pareto solution \mathbf{x} , $\mathbf{y} = \mathbf{f}(\mathbf{x}) \in \mathbb{R}^m$ is called a **Pareto objective**. δ -dominance (Zuluaga et al., 2016) extends the concept of dominance, where the solution $\mathbf{x}^{(a)}$ δ -dominates $\mathbf{x}^{(b)}$ if $(\mathbf{f}(\mathbf{x}^{(a)}) - \delta)$ dominates $\mathbf{f}(\mathbf{x}^{(b)})$. Additionally, a solution \mathbf{x} is called **weakly Pareto optimal** if it cannot be strictly dominated by other solutions ($f_i(x') < f_i(x)$ for all $x' \in \mathcal{X}$).

It is very difficult to optimize all m objectives directly due to their conflicting nature. A more practical approach is to convert the objective vector $\mathbf{f}(\mathbf{x})$ into a single objective problem through an aggregation function $g(\cdot, \boldsymbol{\lambda})$ with a specific weight $\boldsymbol{\lambda}$. Many aggregation methods have been proposed in the past few decades, and this work focuses on the modified Tchebycheff (“mtche” in short) aggregation function (Ma et al., 2017):

$$g^{\text{mtche}}(\mathbf{y}, \boldsymbol{\lambda}) = \max_{i \in [m]} \left(\frac{y_i - z_i}{\lambda_i} \right) : \Delta_{m-1} \mapsto \mathbb{R}^n, \quad (2)$$

where Δ_{m-1} denotes the $m-1$ weight simplex, defined as $\Delta_{m-1} = \{\mathbf{y} | \sum_{i=1}^m y_i = 1, y_i \geq 0\}$. Additionally, let \mathbf{z} be an ideal point such that $z_i \leq f_i(\mathbf{x})$ for all $\mathbf{x} \in \mathcal{X}$.

One attractive property of this aggregation function is that minimizing it produces $\boldsymbol{\lambda}$ -exact Pareto solutions (Mahapatra & Rajan, 2020) under mild conditions (Zhang et al., 2023), namely, for any given $\boldsymbol{\lambda}$, the optimal Pareto objective \mathbf{y}^* , i.e., the minimize of in equation (2), follows the pattern $\left(\frac{y_i^* - z_i}{\lambda_i} \right) = C$, for all $i \in [m]$, where C is a positive constant (vector $\mathbf{y} - \mathbf{z}$ is parallel to $\boldsymbol{\lambda}$).

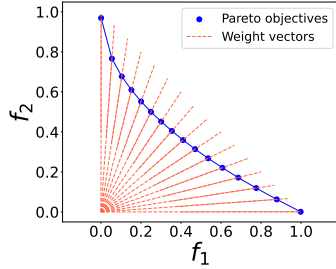


Figure 2. Exact Pareto solutions are intersections between PF and weight vectors.

3. Related work

This section reviews two closely related lines of research. The first is Pareto set learning, which utilizes a single neural model to represent the entire Pareto set. The second is gradient-based methods that aim to find a set of Pareto optimal solutions.

3.1. Pareto set learning

Pareto set learning (PSL) aims to learn the entire Pareto set through a single neural model $x_\beta(\cdot) : \Delta_{m-1} \mapsto \mathbb{R}^n$, where β are the trainable vectors (Navon et al., 2020; Lin et al., 2022; Chen & Kwok, 2022). A PSL model $x_\beta(\cdot)$ is

typically trained by optimizing the following loss function:

$$\min_{\beta} \text{psl_loss}(\beta) = \min_{\beta} \mathbb{E}_{\boldsymbol{\lambda} \sim \text{Unif}(\Delta_{m-1})} [g(\mathbf{f} \circ x_\beta(\boldsymbol{\lambda}), \boldsymbol{\lambda})], \quad (3)$$

where $g(\cdot)$ is some aggregation functions. The gradient involved in Equation (3) is computed by the chain rule: $\nabla_{\beta} \text{psl_loss}(\beta) = \mathbb{E}_{\boldsymbol{\lambda} \sim \text{Unif}(\Delta_{m-1})} \frac{\partial g}{\partial \mathbf{f}} \frac{\partial \mathbf{f}}{\partial \mathbf{x}} \frac{\partial \mathbf{x}}{\partial \beta}$. Since Equation (3) is trained by stochastic gradient descent. Previous PSL methods could fail to find the globally optimal model $x_\beta(\cdot)$ when the objective $\mathbf{f}(\cdot)$ has many local optimas. Another shortcoming of PSL is that the model can become excessively large when the decision space \mathbb{R}^n is large, despite the effective dimension of a Pareto set being only $m-1$ (Zhang et al., 2008). This results in inefficient utilization of the model.

3.2. Gradient-based MOO methods

Gradient-based MOO methods are efficient for optimizing conflicting objectives by utilizing gradient information. However, these methods may get stuck in local Pareto solutions, also known as Pareto stationary solutions. Some notable works in this area include:

1. MOO-SVGD (Liu et al., 2021b): This approach employs Stein Variational Gradient Descent to obtain a diverse set of Pareto solutions.
2. EPO (Mahapatra & Rajan, 2020), COSMOS (Ruchte & Grabocka, 2021), WC-MGDA (Momma et al., 2022), and OPT-in-Pareto (Ye & Liu, 2022): These methods focus on finding a single Pareto solution that satisfies specific user requirements.

However, gradient-based MOO methods often struggle to produce globally optimal solutions. For instance, in the ZDT4 testing problem (Deb et al., 2006), numerous local optimal solutions are present, making it challenging to identify them using gradient information (cf Appendix C.5 for a concrete example). The proposed method is an evolutionary-based approach that does not rely on gradient information to directly optimize objective functions. This characteristic makes it more suitable for finding global optimal solutions and avoids the limitations of gradient-based methods.

4. The proposed UMOEA/D method

In this section, we introduce UMOEA/D, a method for recovering uniform Pareto objectives within the MOEA/D framework. In the MOEA/D framework, decision makers choose a set of diverse weight vectors with the goal of obtaining a diverse set of weight vectors. Various approaches have been proposed to generate diverse weight vectors (Deb et al., 2019; Blank et al., 2020; Das & Dennis, 1998; Tan et al., 2013). A key observation in this paper is that, despite

the diversity of the chosen weight vectors, there exists a *bottleneck* towards achieving the uniform Pareto objectives that decision makers are truly interested in. In the next subsection, we will study the underlying weight-to-objective function, which represents the bottleneck in achieving the desired uniform Pareto objectives.

4.1. Weight-to-objective function and induced Pareto objective distribution

We study the weight-to-objective function with the ‘mtche’ aggregation function (Equation (2)). $\mathbf{h}(\boldsymbol{\lambda}) : \Omega \mapsto \mathbb{R}^m$, which maps a weight $\boldsymbol{\lambda}$ from a weight space to objective space. Here $\mathbf{h}(\boldsymbol{\lambda})$ is defined as.

$$\mathbf{y} = \mathbf{h}(\boldsymbol{\lambda}) = \arg \min_{\mathbf{y}' \in \mathcal{Y}} g^{\text{mtche}}(\mathbf{y}', \boldsymbol{\lambda}). \quad (4)$$

In Equation (4), \mathcal{Y} represents the full feasible objective space, which is the result of mapping the decision space \mathcal{X} through the vector mapping function \mathbf{f} . $\mathcal{Y} = \{\mathbf{f}(x) | x \in \mathcal{X}\}$. To ensure the well-definedness of $\mathbf{h}(\boldsymbol{\lambda})$, the optimal solution \mathbf{y} that minimizes the problem in Equation (4) must be unique. This uniqueness can be achieved by utilizing various methods, including selecting the optimal solution based on lexicographic order. For simplicity, we assume that the original MOP (Equation (1)) does not have any weakly Pareto optimal solutions, which is commonly adopted (Roy et al., 2023; Bergou et al., 2021). Under this assumption, the optimal solution is proven to be unique (cf Corollary A.5 in Appendix A.1). We next build the diffeomorphism of $\mathbf{h}(\boldsymbol{\lambda})$ under the following ‘full mapping’ assumption.

Assumption 4.1 (Full mapping). For each $\boldsymbol{\lambda}$, there exist a scalar k , such that $k\boldsymbol{\lambda} + \mathbf{z}$ is a Pareto objective for the original MOP (Equation (1)), where \mathbf{z} is a reference point used in Equation (2).

This assumption means that for any user preference $\boldsymbol{\lambda}$, there exist a Pareto objective at the ray of vector $\boldsymbol{\lambda}$, which is a common case for example such as famous DTLZ 1-4 testing problems (Deb et al., 2002b). This assumption directly yields the diffeomorphism of $\mathbf{h}(\boldsymbol{\lambda})$ when objectives f_i ’s are differentiable.

Lemma 4.2 (Diffeomorphism of $\mathbf{h}(\boldsymbol{\lambda})$). *Under the Assumption 4.1, if the objectives f_i ’s are differentiable, then the weight-to-objective function $\mathbf{y} = \mathbf{h}(\boldsymbol{\lambda})$ is a diffeomorphism.*

The proof is left in Appendix B. Now we are ready to describe the distribution on the PF. We let $\Lambda_N = \{\boldsymbol{\lambda}^{(1)}, \dots, \boldsymbol{\lambda}^{(N)}\}$ to represent a uniform weight set solving the following weight generating problem as proposed in (Blank et al., 2020),

$$\max_{\Lambda_N \subset \Omega} \min_{\boldsymbol{\lambda}^{(i)}, \boldsymbol{\lambda}^{(j)} \in \Lambda_N} \rho(\boldsymbol{\lambda}^{(i)}, \boldsymbol{\lambda}^{(j)}).$$

The asymptotic Pareto objectives distribution is given by the following theorem:

Theorem 4.3. *The category distribution $\tilde{\mathbf{Y}}_N$ over a set of Pareto objectives $\mathbf{Y}_N = \{\mathbf{y}^{(1)}, \dots, \mathbf{y}^{(N)}\}$ converges in distribution to $\mathbf{h} \circ \text{Unif}(\Omega)$, denoted as $\tilde{\mathbf{Y}}_N \xrightarrow{d} \mathbf{h} \circ \text{Unif}(\Omega)$, where $\mathbf{y}^{(i)} = \mathbf{h}(\boldsymbol{\lambda}^{(i)})$, and the probability density function (pdf) of $\tilde{\mathbf{Y}}_N$ converges to $\frac{1}{A} \text{Det}(\mathbf{J}(\mathbf{h}^{-1}))$. Here $A = \mathcal{H}_{m-1}(\Omega)$ represents the Hausdorff measure for a $(m-1)$ -dimensional manifold, and \mathbf{J} is the Jacobian matrix*

The term $\text{Unif}(\Omega)$ denotes the uniform distribution over the set Ω . The proof is in Appendix D.5.

We observe from Theorem 4.3 that generating uniform Pareto objectives is challenging due to the non-linearity of the function $\mathbf{h}(\boldsymbol{\lambda})$. To illustrate this point, we present concrete results for widely used multiobjective ZDT (Deb et al., 2006) and DTLZ (Deb et al., 2002a) problems when the weight space is selected as simplexes.

1. ZDT1: $y_1 = k\lambda_1$, $y_2 = k(1 - \sqrt{\lambda_1})$, where $k = \frac{2 - \lambda_1 - \sqrt{-3\lambda_1^2 + 4\lambda_1}}{2(\lambda_1 - 1)^2}$.
2. ZDT2: $y_1 = k\lambda_1$, $y_2 = k(1 - \lambda_1^2)$, where $k = \frac{\lambda_1 - 1 + \sqrt{5\lambda_1^2 - 2\lambda_1 + 1}}{2\lambda_1^2}$.
3. DTLZ1: $f_i = 0.5\lambda_i$, for $i = 1, 2, 3$.

From these examples, we observe that uniformity in the weight space does not always imply uniformity in the Pareto objective space, except in specific circumstances when $\mathbf{h}(\boldsymbol{\lambda})$ is an affine mapping, as is the case for DTLZ1.

4.2. UMOEA/D framework

As discussed in the previous section, achieving a uniform Pareto objective is challenging due to the non-linearity of the weight-to-objective function $\mathbf{h}(\boldsymbol{\lambda})$. To attain uniformity on the PF, two key steps need to be taken. First, it is necessary to formally define what is ‘uniformity’ for a MOP. Second, it is crucial to model $\mathbf{h}(\boldsymbol{\lambda})$, and therefore, we are able find those particular weight vectors resulting in uniform Pareto objectives.

We begin by analyzing the concept of uniformity in the context of multiobjective optimization problems. We provide two precise definitions of uniformity, starting with the asymptotic definition:

Definition 4.4 (Asymptotic uniformity on PF, adapted from (Borodachov et al., 2007)[Eq. 1.10].) We say a series of set \mathbf{Y}_N to be asymptotically uniform on \mathcal{T} (the PF) with respect to the Hausdorff measure \mathcal{H}_{m-1} if, for any subset $\mathcal{B} \subset \mathcal{T}$ with a boundary having a \mathcal{H}_{m-1} -measure of zero,

the following condition holds:

$$\lim_{N \rightarrow \infty} \frac{\text{Card}(\mathbf{Y}_N \cap \mathcal{B})}{\text{Card}(\mathbf{Y}_N)} = \frac{\mathcal{H}_{m-1}(\mathcal{B})}{\mathcal{H}_{m-1}(\mathcal{T})}, \quad (5)$$

where Card represents the cardinality function. For example, $\text{Card}(\mathbf{Y}_N \cap \mathcal{B})$ indicates the number of points in \mathbf{Y}_N that belong to \mathcal{B} .

Intuitively, this definition implies that as the number of solutions in set \mathbf{Y}_N tends to infinity, for any subset \mathcal{B} with a boundary having a \mathcal{H}_{m-1} -measure of zero, the ratio of solutions lying in set \mathcal{B} is equal to the ratio of the cardinality of \mathcal{B} to the cardinality of the entire PF. In other words, it suggests that the solutions in \mathbf{Y}_N must be uniformly distributed on the PF. The second definition is for the non-aymtotic case,

Definition 4.5 (Non-asymptotic uniformity on PF). We say a set \mathbf{Y}_N is non-asymptotically uniform on \mathcal{T} with a parameter $\delta > 0$ when for any Pareto objective $\mathbf{y} \in \mathcal{T}$, there exist a objective $\mathbf{y}' \in \mathbf{Y}_N$ such that, $\rho(\mathbf{y}, \mathbf{y}') \leq \delta$.

The non-asymptotic definition implies that for an arbitrary Pareto objective \mathbf{y} , there exists a solution \mathbf{y}' in the discrete set \mathbf{Y}_N such that \mathbf{y}' is an approximation of \mathbf{y} with an error of at most δ . When the value of δ is small, the set \mathbf{Y}_N serves as a suitable representation of the PF.

To generate uniformly distributed Pareto objectives, we propose to construct the objective configuration \mathbf{Y}_N by solving the Maximal-Manifold-Separation (MMS) problem on the PF,

$$\max_{\mathbf{Y}_N} \delta = \max_{\mathbf{Y}_N} \left(\min_{\mathbf{y}^{(i)} \neq \mathbf{y}^{(j)} \in \mathbf{Y}_N \subset \mathcal{T}} \rho(\mathbf{y}^{(i)}, \mathbf{y}^{(j)}) \right). \quad (6)$$

Intuitively, Equation (6) maximizes the minimum pairwise distances among all Pareto objectives. This objective ensures that densely populated solutions are spread apart, leading to a uniform distribution of Pareto objectives. We denote the optimal configuration of Equation (6) as \mathbf{Y}_N^* with a separation parameter of δ^* . \mathbf{Y}_N^* exhibits the following attractive uniform properties.

Proposition 4.6. ① Under mild conditions, \mathbf{Y}_N^* is non-asymptotically uniform on \mathcal{T} with a parameter of δ^* . ② \mathbf{Y}_N^* is asymptotically uniform on \mathcal{T} when \mathcal{T} is both compact and connected.

Please refer to Appendix D.3 for the conditions and missing proofs. After those definitions, we introduce a compact framework for searching for uniform Pareto objectives in the MOEA/D framework. Since the true PF is unknown, we iteratively estimates the PF by learning the mapping from weight vectors to Pareto objectives. With the estimated PF, we then select weight vectors that exhibit the highest

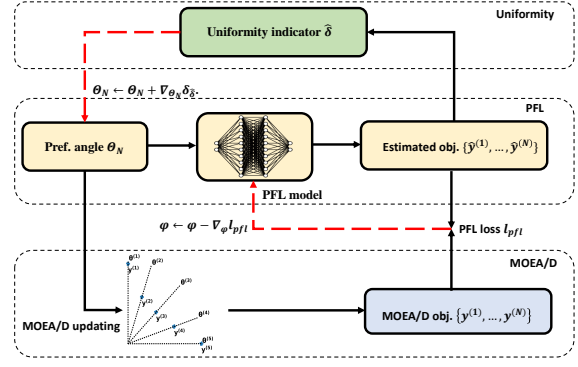


Figure 3. UMOEA/D consists of three parts: training the PFL model, updating new weights and MOEA/D. Firstly, Pareto optimal solutions are solved under initial weight vectors. Then, we use those weight vector and Pareto objective pairs to train a PFL model. Finally, new weight vectors are optimized by this model for achieving the most uniform Pareto objectives. Those three steps are performed iteratively.

Table 1. Comparison of model size between PSL and PFL. Note that for practical problems, decision variables n is usually much larger than m .

Method	Mapping function
Pareto Set Learning (PSL)	$\Delta_{m-1} \mapsto \mathbb{R}^n$
Pareto Front Learning (PFL)	$[0, \frac{\pi}{2}]^{m-1} \mapsto \mathbb{R}^m$

level of uniformity in their corresponding Pareto objectives. The framework comprises multiple components, and the computation flow is depicted in Figure 3.

① We represent weight vectors using a set of weight angles $\Theta_N = [\theta^{(1)}, \dots, \theta^{(N)}]$. They are converted to each other by Equation (13) and Equation (14) in Appendix. One advantage of using weight angles is the simple constraint shape of each $\theta^{(i)} \in [0, \frac{\pi}{2}]^{m-1}$. In contrast, a weight vector is constrained on a simplex, which is more challenging to handle. A MOEA/D frame accept a set of weight angles and optimize for the Pareto objectives \mathbf{Y}_N . ② The Pareto Front Learning (PFL) module is then trained using the true objectives obtained from the output of MOEA/D. ③ Subsequently, the weight angles are updated for achieving the most uniform Pareto objectives.

More detailed descriptions of ② the PFL model and ③ the weight update components are provided separately in the subsequent sections. The practical algorithm is implemented as Algorithm 1 and 2 in Appendix B.3, where we also present time complexity analysis.

4.3. Pareto front learning (PFL)

The PFL model, $\mathbf{h}_\phi(\cdot) : [0, \frac{\pi}{2}]^{m-1} \mapsto \mathbb{R}^m$, approximates the weight-to-objective function $\mathbf{h}(\boldsymbol{\lambda})$ discussed in Section 4.1. It predicts the Pareto objective optimized by the modified Tchebycheff function under a specific weight angle $\boldsymbol{\theta}$. $\mathbf{h}_\phi(\cdot)$ is trained by minimizing the mean square error (MSE) loss between the true Pareto objectives \mathbf{y} from MOEA/D and the estimated objectives $\mathbf{h}_\phi(\boldsymbol{\theta})$. In practice, the training time of the PFL model is fast (less than 1s) and can be neglected compared to other operations in a multiobjective evolutionary algorithm.

We emphasize the necessity of introducing $\mathbf{h}_\phi(\cdot)$ rather than simply applying previous Pareto set learning methods, which learn the mapping from weight space to solution space \mathbb{R}^n (Navon et al., 2020; Lin et al., 2022). ① PSL simply uses gradient-based methods to optimize the PSL objective function defined in Equation (3). The induced locally optimal solutions make PSL fail on most MOEA benchmarks like ZDT, DTLZ problems. ② In an MOO problem, the number of decision variables n can be arbitrarily large, while the efficient dimension of a Pareto set is only $m-1$ (Zhang et al., 2008). PSL fails to detect it, resulting in the output of an n -D solution, leading to potentially large PSL model size. In contrast, the PFL model is constrained in the function space $[0, \frac{\pi}{2}]^{m-1} \mapsto \mathbb{R}^m$, which implies its complexity is independent of n .

4.4. Weight adjustment with a PFL model

Solving the optimal configuration (Equation (6)) on the PF with an arbitrary set size N , is generally a NP-hard problem (Borodachov et al., 2019). Therefore, we propose a parameterized problem to approximate problem (Equation (6)). Notice that, when the PFL model \mathbf{h}_ϕ is trained, $\hat{\mathcal{T}} = \{\mathbf{h}_\phi(\boldsymbol{\theta}) | \boldsymbol{\theta} \in [0, \frac{\pi}{2}]^{m-1}\}$ is a good approximator of the true PF. We further show the average error of $\hat{\mathcal{T}}$ and \mathcal{T} is bounded in the empirical risk and maximal pairwise distances in Remark 4.9. Solving the optimal weight factors which lead to uniform distribution on the estimated PF can be formulated as the following problem,

$$\max_{\Theta_N} \hat{\delta} = \max_{\Theta_N} \left(\min_{1 \leq i < j \leq N} \rho(\mathbf{h}_\phi(\boldsymbol{\theta}^{(i)}), \mathbf{h}_\phi(\boldsymbol{\theta}^{(j)})) \right) \quad (7)$$

After this replacement, the parameterized optimization problem can be solved efficiently by projected gradient ascent

method

$$\boldsymbol{\theta}^{(i)} \leftarrow \text{Proj}(\boldsymbol{\theta}^{(i)} + \eta \nabla_{\boldsymbol{\theta}^{(i)}} \hat{\delta}), \quad i \in [N],$$

where η is a learning rate and the Proj operator projects a weight angle back to its domain $[0, \frac{\pi}{2}]^{m-1}$.

Figure 4 demonstrates that a PFL model can effectively estimate the whole PF well with only a few numbers of Pareto objectives. The blue dots represent the original Pareto objectives optimized by MOEA/D, while the red stars are Pareto objectives after weight adjustment.

4.5. PFL generalization bound

As discussed in Appendix D.1, the population can be controlled by bounding this generalization error. We discuss the PFL generalization error, namely $\tilde{\epsilon} = |R(\tilde{\mathbf{h}}) - \hat{R}(\tilde{\mathbf{h}})|$ for an arbitrary diffeomorphic $\tilde{\mathbf{h}}(\cdot)$, where $R(\cdot)/\hat{R}(\cdot)$ denote the population and empirical risks respectively.

Theorem 4.7 (PFL Generalization Bound). *We first make some regularity assumptions:*

- (Function smoothness). Both $(\tilde{\mathbf{h}} - \mathbf{h}_*)(\cdot)$ and $\mathbf{h}_*^{-1}(\cdot)$ are L - and L' -Lipschitz, respectively, ie $\forall \boldsymbol{\theta}^{(1)}, \boldsymbol{\theta}^{(2)} \in [0, \frac{\pi}{2}]^{m-1}$ and $\forall \mathbf{y}^{(1)}, \mathbf{y}^{(2)} \in \mathbb{R}^m$,

$$\begin{aligned} \|\tilde{\mathbf{h}}(\boldsymbol{\theta}^{(1)}) - \tilde{\mathbf{h}}(\boldsymbol{\theta}^{(2)})\| &\leq L \|\boldsymbol{\theta}^{(1)} - \boldsymbol{\theta}^{(2)}\|, \\ \|\mathbf{h}_*^{-1}(\mathbf{y}^{(1)}) - \mathbf{h}_*^{-1}(\mathbf{y}^{(2)})\| &\leq L' \|\mathbf{y}^{(1)} - \mathbf{y}^{(2)}\|, \end{aligned} \quad (8)$$

where \mathbf{h}_* denotes the true mapping function from weights to objectives.

- (Function bound). $\|\tilde{\mathbf{h}} - \mathbf{h}_*\|_\infty \leq A$, $\|\mathbf{h}_*^{-1}\|_\infty \leq A'$. The function \mathbf{h}^{-1} exists according to Lemma 4.2.
- (Manifold property). We assume \mathcal{T} is a differentiable, compact $(m-1)$ -D manifold, a common assumption (Hillermeier, 2001; Roy et al., 2023). We also assume \mathcal{T} is connected which is common.

Under the above assumptions, for the risk $\tilde{\epsilon} = |R(\tilde{\mathbf{h}}) - \hat{R}(\tilde{\mathbf{h}})|$, we have the following bound,

$$\tilde{\epsilon} \leq 2\mathcal{H}_{m-1}(\mathcal{T})AA'LL'\delta_v + 2CA^2\sqrt{\mathcal{W}_1(\mathcal{U}, \tilde{\mathbf{Y}}_N) + \delta_v}, \quad (9)$$

where \mathcal{U} is the uniform distribution over \mathcal{T} , $\tilde{\mathbf{Y}}_N$ is the empirical distribution of \mathbf{Y} , $\mathcal{W}_1(\cdot, \cdot)$ is the Wasserstein distance with the ℓ_1 norm, δ_v represents the maximal diameter of Voronoi cells¹, and C is some universal constant representing the smoothness of \mathcal{T} (Chae & Walker, 2020). We left the proof in Appendix D.2.

Remark 4.8. In Theorem 4.7, the error bound for $\tilde{\epsilon}$ involves two quantities, the diameter of the Voronoi cell δ_v and

¹For the formal definition of Voronoi cells and diameter of a set, please refer to Definitions B.4 and B.5

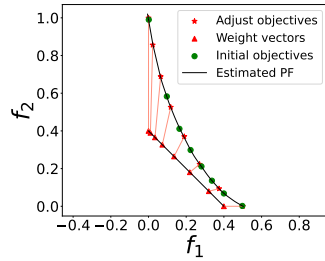


Figure 4. Weight adjustment.

Table 2. The running time (every 1k generations) of SMS-EMOA, PaLam, and UMOEA/D.

Running Time (minutes)	DTLZ2	RE37	RE41	RE42
SMS-EMOA	1.21	3.23	24.12	18.76
PaLam	0.72	1.59	7.69	6.05
UMOEAD	0.56	0.71	2.48	2.55

Wasserstein distance $\mathcal{W}_1(\mathcal{U}, \tilde{\mathcal{Y}}_N)$. The margin δ_v is controlled by maximizing the minimal separation distance. The decaying rate of $\mathcal{W}_1(\mathcal{U}, \tilde{\mathcal{Y}}_N)$ is impacted by not only the margin δ_v , but also the manifold properties of the PF. However, by Proposition 4.6-②, we still have $\mathcal{W}_1(\mathcal{U}, \tilde{\mathcal{Y}}_N) \rightarrow 0$ since $\tilde{\mathcal{Y}}_N$ weakly converges to \mathcal{U} , and minimizing the margin δ_v is thus critical to the control of the generalization error $\tilde{\epsilon}$.

Remark 4.9 (Average PF estimation error). $R(\tilde{h})$ equals to $\int_{[0, \frac{\pi}{2}]^{m-1}} \|\tilde{h}(\theta) - h_*(\theta)\| d\theta$, the average error of $\tilde{\mathcal{T}}$ and \mathcal{T} . Hence, this average error can accordingly be upper bounded by $\tilde{\epsilon} + \hat{R}(\tilde{h})$.

5. Experiments

5.1. Experiment settings

We validate the effectiveness of the proposed method on various MOEA problems, including ZDT1,2,4,6 (Deb et al., 2006) (PFs of ZDT3,5 are disconnected thus not included), DTLZ 1-4 (Deb et al., 2002b), and real-world problems, namely, four-bar truss design (RE21), reinforced concrete beam design (RE22), rocket injector design (RE37), car side impact design (RE41), and conceptual marine design (RE42) (Tanabe & Ishibuchi, 2020). RE41 and RE42 are four-objective problems owning a very large objective space, and the previous method is very difficult to cover the PF efficiently.

For presentation, we normalize the PF of RE37/RE41/RE42 to $[0, 1]^3$. To test the ability to deal with objectives of different scales, the PFs of RE21 and RE22 are normalized to $[0, 0.5] \times [0, 1]$. ZDTs and DTLZs possess numerous local optima that cannot be identified by gradient-based MOO methods (see Appendix C.5). The RE problems are real-world problems with unknown PFs.

The implementation in this study relies on the pymoo (Blank & Deb, 2020) and PyTorch (Paszke et al., 2019) libraries. We use the simulated binary crossover operator (SBX) and the polynomial mutation technique (Deb & Beyer, 2001) for MOEA/D-based methods. Following the pymoo setting, we do not maintain an external population (EP), as it can be computationally and storage intensive (Li & Landa-Silva, 2011).

We compare our method with ① vanilla MOEA/D (Zhang

& Li, 2007), ② MOEA/D with adaptive weight adjustment (MOEA/D-AWA) (Qi et al., 2014; de Farias et al., 2018), ③ PaLam (Siwei et al., 2011), ④ SMS-EMOA (Beume et al., 2007), ⑤ MOEA/Ds adjustment with linear-segment (Dong et al., 2020) (MOEA/D-L), and ⑥ MOEA/D-GP (Wu et al., 2017). SMS-EMOA and PaLam are hypervolume-based method. Though there are many fast hypervolume approximation algorithms, calculate the hypervolume or its gradient is computation inefficient (Guerreiro et al., 2020).

To assess performances, we utilize ① the hypervolume (HV) (\uparrow) (Guerreiro et al., 2020), ② the sparsity (\downarrow) (Xu et al., 2020), ③ the spacing (\downarrow) (Schott, 1995), ④ the minimal distance on the PF (δ) (\uparrow) and its soft version ⑤ ($\tilde{\delta}$) (\uparrow) indicators. Please refer to Appendix C.1 and C.2 for detailed descriptions related methods and indicator details.

Table 3. Results on all problems averaged on five random seeds.

Method	HV	Spacing	Sparsity	δ	$\tilde{\delta}$
RE37					
SMS-EMOA	1.1143	0.0423	0.0052	0.0294	-0.1270
MOEA/D-AWA	1.0768	0.0797	0.0101	0.0012	-0.2055
MOEA/D-GP	1.0737	0.0715	0.0083	0.0023	-0.1723
MOEA/D	1.0519	0.0758	0.0122	0.0000	-0.2055
PaLam	1.1150	0.0712	0.0050	0.0023	-0.1473
UMOEAD	1.1114	0.0416	0.0047	0.0483	-0.0805
RE41					
SMS-EMOA	1.0976	0.0516	0.0014	0.0037	-0.2458
MOEA/D-AWA	1.1432	0.0676	0.0026	0.0000	-0.3001
MOEA/D-GP	1.1694	0.0687	0.0013	0.0001	-0.2798
MOEA/D	1.1328	0.0578	0.0034	0.0000	-0.2998
PaLam	1.2075	0.0551	0.0009	0.0019	-0.2352
UMOEAD	1.2072	0.0436	0.0008	0.0060	-0.1876

5.2. Results Analysis

The average results on five random seeds for *all* problems are displayed in Table 5 and 6 in Appendix C.3, along with the visualization results in Figure 6-11. Due to page limit, we report on three representative results on RE37, RE41, RE42 in the main paper. We ablate in Appendix C.5 that only using gradient information easily lead to a local optimal solution.

The proposed method achieves the optimal spacing indicator. For two-objective problems, the spacing indicator is very close to zero, indicating that the distances between adjacent solutions are nearly equal. We observed that HV-based methods such as SMS-EMOA and PaLam generated more diverse solutions compared to the vanilla MOEA/D. The main reason for this is that, in many real-world problems, numerous weight vectors do not intersect with the PF, resulting in duplicate Pareto solutions. This duplication wastes computation resources. UMOEA/D addresses the issue of duplicate Pareto objectives through adaptive weight adjustment. By aiming to maximize the minimal separation, UMOEA/D avoids generating duplicate Pareto solutions, as duplicate solutions would automatically have a minimal

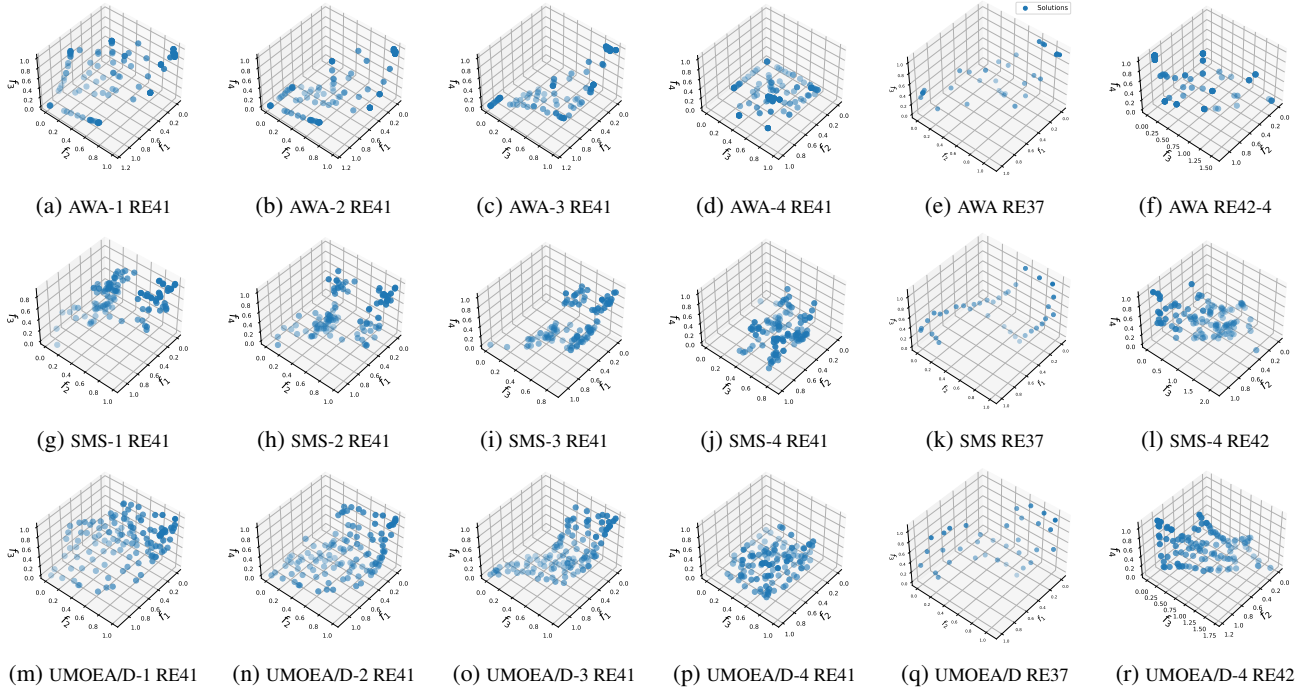


Figure 5. Experimental results on the three-objective RE37 and four-objective RE41/RE42 problems. Here, the “Method- i , $i = 1, 2, 3, 4$ ” notation refers to the projection of the objectives on the objective space (f_1, f_2, f_3) , (f_1, f_2, f_4) , (f_1, f_3, f_4) , and (f_2, f_3, f_4) , respectively.

distance of zero.

Contrary to the commonly held belief that hypervolume-based methods yield diverse solutions (Auger et al., 2012; Guerreiro et al., 2020), our findings reveal that hypervolume indicators can be very similar, while the distribution of solutions can vary significantly. This means that adopting a novel indicator in MOO to accurately measure the diversity level of solutions, as proposed, is necessary. Figure 5(k) shows that hypervolume-based methods tend to generate solutions on the boundary of the PF and lack guarantees of δ -dominance. In contrast, UMOEA/D generates uniformly distributed Pareto objectives more effectively than hypervolume-based methods across most problems. Another notable advantage of UMOEA/D over hypervolume-based methods is the computational efficiency it offers. Computation of the hypervolume for a 3/4 objective problem can be expensive, while solving MOEA/D subproblems can be parallelized, leading to highly efficient computations. This advantage is supported by the results presented in Table 2, demonstrating that UMOEA/D successfully achieves approximately a great $10\times$ speed improvement compared to SMS-EMOA and a $3\times$ speed improvement compared to PaLam.

UMOEA/D offers a notable advantage over other weight adjustment methods, such as MOEA/D-AWA (Qi et al.,

2014; de Farias et al., 2018), MOEA/D-GP (Wu et al., 2017), and MOEA/D-L (Dong et al., 2020). It excels in accurately modeling the Pareto Front (PF) while providing theoretical guarantees for the level of uniformity. The figure clearly demonstrates this advantage, where UMOEA/D generates significantly more uniformly distributed Pareto objectives for challenging 3/4 objective problems. In comparison, MOEA/D-AWA produces Pareto objectives that are often closely clustered together, resulting in limited coverage across a broad region. Conversely, UMOEA/D consistently generates solutions that span the entire Pareto front.

6. Conclusions and future directions

This paper attempts to address a long-standing problem in MOEAs: the generation of uniformly distributed Pareto objectives to well represent the characteristics of the whole PF. To the best of our knowledge, this is the first paper that rigorously analyzes the distribution of Pareto objectives, and thereby sheds light on the understanding of solution generation in MOEAs. Building upon the theoretical findings, we introduce a novel algorithm that constructs a uniformly distributed Pareto objective set through NN-assisted weight adjustment. We will extend UMOEA/D for large applications such as drug design in our further work.

Broader Impact

As a multiobjective method, our work poses low social risk as its results depend on downstream applications. One use case is building trustworthy AI systems to understand trade-offs between conflicting objectives. Hence, the negative societal impact of our work is unlikely.

References

- Allen-Zhu, Z., Li, Y., and Song, Z. A convergence theory for deep learning via over-parameterization. In *International conference on machine learning*, pp. 242–252. PMLR, 2019.
- Auger, A., Bader, J., Brockhoff, D., and Zitzler, E. Hypervolume-based multiobjective optimization: Theoretical foundations and practical implications. *Theoretical Computer Science*, 425:75–103, 2012.
- Bergou, E.-H., Diouane, Y., and Kungurtsev, V. Complexity iteration analysis for strongly convex multi-objective optimization using a newton path-following procedure. *Optimization Letters*, 15:1215–1227, 2021.
- Bernreuther, M., Dellnitz, M., Gebken, B., Müller, G., Peitz, S., Sonntag, K., and Volkwein, S. Multiobjective optimization of non-smooth pde-constrained problems. *arXiv preprint arXiv:2308.01113*, 2023.
- Beume, N., Naujoks, B., and Emmerich, M. Sms-emoa: Multiobjective selection based on dominated hypervolume. *European Journal of Operational Research*, 181(3):1653–1669, 2007.
- Blank, J. and Deb, K. pymoo: Multi-objective optimization in python. *IEEE Access*, 8:89497–89509, 2020.
- Blank, J., Deb, K., Dhebar, Y., Bandaru, S., and Seada, H. Generating well-spaced points on a unit simplex for evolutionary many-objective optimization. *IEEE Transactions on Evolutionary Computation*, 25(1):48–60, 2020.
- Blank, J., Deb, K., Dhebar, Y., Bandaru, S., and Seada, H. Generating well-spaced points on a unit simplex for evolutionary many-objective optimization. *IEEE Transactions on Evolutionary Computation*, 2020.
- Borodachov, S., Hardin, D., and Saff, E. Asymptotics of best-packing on rectifiable sets. *Proceedings of the American Mathematical Society*, 135(8):2369–2380, 2007.
- Borodachov, S. V., Hardin, D. P., and Saff, E. B. *Discrete energy on rectifiable sets*. Springer, 2019.
- Caramia, M., Dell’Olmo, P., Caramia, M., and Dell’Olmo, P. Multi-objective optimization. *Multi-objective Management in Freight Logistics: Increasing Capacity, Service Level, Sustainability, and Safety with Optimization Algorithms*, pp. 21–51, 2020.
- Chae, M. and Walker, S. G. Wasserstein upper bounds of the total variation for smooth densities. *Statistics & Probability Letters*, 163:108771, 2020.
- Chen, W. and Kwok, J. Multi-objective deep learning with adaptive reference vectors. *Advances in Neural Information Processing Systems*, 35:32723–32735, 2022.
- Das, I. and Dennis, J. E. Normal-boundary intersection: A new method for generating the pareto surface in nonlinear multicriteria optimization problems. *SIAM journal on optimization*, 8(3):631–657, 1998.
- de Farias, L. R., Braga, P. H., Bassani, H. F., and Araújo, A. F. Moea/d with uniformly randomly adaptive weights. In *Proceedings of the genetic and evolutionary computation conference*, pp. 641–648, 2018.
- Deb, K. and Beyer, H.-G. Self-adaptive genetic algorithms with simulated binary crossover. *Evolutionary computation*, 9(2):197–221, 2001.
- Deb, K. and Deb, D. Analysing mutation schemes for real-parameter genetic algorithms. *International Journal of Artificial Intelligence and Soft Computing*, 4(1):1–28, 2014.
- Deb, K., Agrawal, R. B., et al. Simulated binary crossover for continuous search space. *Complex systems*, 9(2):115–148, 1995.
- Deb, K., Pratap, A., Agarwal, S., and Meyarivan, T. A fast and elitist multiobjective genetic algorithm: Nsga-ii. *IEEE transactions on evolutionary computation*, 6(2):182–197, 2002a.
- Deb, K., Thiele, L., Laumanns, M., and Zitzler, E. Scalable multi-objective optimization test problems. In *Proceedings of the 2002 Congress on Evolutionary Computation. CEC’02 (Cat. No. 02TH8600)*, volume 1, pp. 825–830. IEEE, 2002b.
- Deb, K., Sinha, A., and Kukkonen, S. Multi-objective test problems, linkages, and evolutionary methodologies. In *Proceedings of the 8th annual conference on Genetic and evolutionary computation*, pp. 1141–1148, 2006.
- Deb, K., Bandaru, S., and Seada, H. Generating uniformly distributed points on a unit simplex for evolutionary many-objective optimization. In *Evolutionary Multi-Criterion Optimization: 10th International Conference, EMO 2019, East Lansing, MI, USA, March 10-13, 2019, Proceedings 10*, pp. 179–190. Springer, 2019.

- Dong, Z., Wang, X., and Tang, L. Moea/d with a self-adaptive weight vector adjustment strategy based on chain segmentation. *Information Sciences*, 521:209–230, 2020.
- Durrett, R. *Probability: theory and examples*, volume 49. Cambridge university press, 2019.
- Ehrgott, M. *Multicriteria optimization*, volume 491. Springer Science & Business Media, 2005.
- Elarbi, M., Bechikh, S., Coello, C. A. C., Makhlof, M., and Said, L. B. Approximating complex pareto fronts with predefined normal-boundary intersection directions. *IEEE Transactions on Evolutionary Computation*, 24(5): 809–823, 2019.
- Folland, G. B. *Real analysis: modern techniques and their applications*, volume 40. John Wiley & Sons, 1999.
- Guerreiro, A. P., Fonseca, C. M., and Paquete, L. The hypervolume indicator: Problems and algorithms. *arXiv preprint arXiv:2005.00515*, 2020.
- Hayes, C. F., Rădulescu, R., Bargiacchi, E., Källström, J., Macfarlane, M., Reymond, M., Verstraeten, T., Zintgraf, L. M., Dazeley, R., Heintz, F., et al. A practical guide to multi-objective reinforcement learning and planning. *Autonomous Agents and Multi-Agent Systems*, 36(1):26, 2022.
- Hillermeier, C. Generalized homotopy approach to multiobjective optimization. *Journal of Optimization Theory and Applications*, 110(3):557–583, 2001.
- Hu, Y., Xian, R., Wu, Q., Fan, Q., Yin, L., and Zhao, H. Revisiting scalarization in multi-task learning: A theoretical perspective. *arXiv preprint arXiv:2308.13985*, 2023.
- Jiao, R., Zeng, S., Li, C., and Ong, Y.-S. Two-type weight adjustments in moea/d for highly constrained many-objective optimization. *Information Sciences*, 578: 592–614, 2021.
- Li, H. and Landa-Silva, D. An adaptive evolutionary multi-objective approach based on simulated annealing. *Evolutionary computation*, 19(4):561–595, 2011.
- Li, K., Deb, K., Zhang, Q., and Kwong, S. An evolutionary many-objective optimization algorithm based on dominance and decomposition. *IEEE transactions on evolutionary computation*, 19(5):694–716, 2014.
- Liang, J., Gong, K., Li, S., Liu, C. H., Li, H., Liu, D., Wang, G., et al. Pareto domain adaptation. *Advances in Neural Information Processing Systems*, 34:12917–12929, 2021.
- Lin, X., Zhen, H.-L., Li, Z., Zhang, Q.-F., and Kwong, S. Pareto multi-task learning. *Advances in neural information processing systems*, 32, 2019.
- Lin, X., Yang, Z., and Zhang, Q. Pareto set learning for neural multi-objective combinatorial optimization. *arXiv preprint arXiv:2203.15386*, 2022.
- Liu, D., Qi, Y., Yang, R., Quan, Y., Li, X., and Miao, Q. A tri-objective preference-based uniform weight design method using delaunay triangulation. *Soft Computing*, 25(15):9703–9729, 2021a.
- Liu, X., Tong, X., and Liu, Q. Profiling pareto front with multi-objective stein variational gradient descent. *Advances in Neural Information Processing Systems*, 34: 14721–14733, 2021b.
- Ma, X., Zhang, Q., Tian, G., Yang, J., and Zhu, Z. On tchebycheff decomposition approaches for multiobjective evolutionary optimization. *IEEE Transactions on Evolutionary Computation*, 22(2):226–244, 2017.
- Mahapatra, D. and Rajan, V. Multi-task learning with user preferences: Gradient descent with controlled ascent in pareto optimization. In *International Conference on Machine Learning*, pp. 6597–6607. PMLR, 2020.
- Miettinen, K. *Nonlinear multiobjective optimization*, volume 12. Springer Science & Business Media, 1999.
- Momma, M., Dong, C., and Liu, J. A multi-objective/multi-task learning framework induced by pareto stationarity. In *International Conference on Machine Learning*, pp. 15895–15907. PMLR, 2022.
- Navon, A., Shamsian, A., Chechik, G., and Fetaya, E. Learning the pareto front with hypernetworks. *arXiv preprint arXiv:2010.04104*, 2020.
- Okabe, A., Boots, B., Sugihara, K., and Chiu, S. N. *Spatial tessellations: concepts and applications of voronoi diagrams*. 2009.
- Paszke, A., Gross, S., Massa, F., Lerer, A., Bradbury, J., Chanan, G., Killeen, T., Lin, Z., Gimelshein, N., Antiga, L., et al. Pytorch: An imperative style, high-performance deep learning library. *Advances in neural information processing systems*, 32, 2019.
- Qi, Y., Ma, X., Liu, F., Jiao, L., Sun, J., and Wu, J. Moea/d with adaptive weight adjustment. *Evolutionary computation*, 22(2):231–264, 2014.
- Rhee, C.-H., Zhou, E., and Qiu, P. Space-filling design for nonlinear models. *arXiv preprint arXiv:1710.11616*, 2017.
- Roy, A., So, G., and Ma, Y.-A. Optimization on pareto sets: On a theory of multi-objective optimization. *arXiv preprint arXiv:2308.02145*, 2023.

- Ruchte, M. and Grabocka, J. Scalable pareto front approximation for deep multi-objective learning. In *2021 IEEE international conference on data mining (ICDM)*, pp. 1306–1311. IEEE, 2021.
- Schott, J. R. Fault tolerant design using single and multicriteria genetic algorithm optimization. 1995.
- Schulz, A., Xu, J., Zhu, B., Zheng, C., Grinspun, E., and Matusik, W. Interactive design space exploration and optimization for cad models. *ACM Transactions on Graphics (TOG)*, 36(4):1–14, 2017.
- Siwei, J., Zhihua, C., Jie, Z., and Yew-Soon, O. Multiobjective optimization by decomposition with pareto-adaptive weight vectors. In *2011 Seventh international conference on natural computation*, volume 3, pp. 1260–1264. IEEE, 2011.
- Tan, Y.-Y., Jiao, Y.-C., Li, H., and Wang, X.-K. A modification to moea/d-de for multiobjective optimization problems with complicated pareto sets. *Information Sciences*, 213:14–38, 2012.
- Tan, Y.-Y., Jiao, Y.-C., Li, H., and Wang, X.-K. Moea/d+ uniform design: A new version of moea/d for optimization problems with many objectives. *Computers & Operations Research*, 40(6):1648–1660, 2013.
- Tanabe, R. and Ishibuchi, H. An easy-to-use real-world multi-objective optimization problem suite. *Applied Soft Computing*, 89:106078, 2020.
- Telgarsky, M. Deep learning theory lecture notes. <https://mjt.cs.illinois.edu/dlt/>, 2021. Version: 2021-10-27 v0.0-e7150f2d (alpha).
- Vershynin, R. *High-dimensional probability: An introduction with applications in data science*, volume 47. Cambridge university press, 2018.
- Wang, L., Ng, A. H., and Deb, K. *Multi-objective evolutionary optimisation for product design and manufacturing*. Springer, 2011.
- Wu, M., Kwong, S., Jia, Y., Li, K., and Zhang, Q. Adaptive weights generation for decomposition-based multi-objective optimization using gaussian process regression. In *Proceedings of the Genetic and Evolutionary Computation Conference*, pp. 641–648, 2017.
- Xian, R., Yin, L., and Zhao, H. Fair and optimal classification via post-processing. In *International Conference on Machine Learning*, pp. 37977–38012. PMLR, 2023.
- Xu, J., Tian, Y., Ma, P., Rus, D., Sueda, S., and Matusik, W. Prediction-guided multi-objective reinforcement learning for continuous robot control. In *International conference on machine learning*, pp. 10607–10616. PMLR, 2020.
- Xu, J., Spielberg, A., Zhao, A., Rus, D., and Matusik, W. Multi-objective graph heuristic search for terrestrial robot design. In *2021 IEEE international conference on robotics and automation (ICRA)*, pp. 9863–9869. IEEE, 2021.
- Ye, M. and Liu, Q. Pareto navigation gradient descent: a first-order algorithm for optimization in pareto set. In *Uncertainty in Artificial Intelligence*, pp. 2246–2255. PMLR, 2022.
- Zhang, Q. and Li, H. Moea/d: A multiobjective evolutionary algorithm based on decomposition. *IEEE Transactions on evolutionary computation*, 11(6):712–731, 2007.
- Zhang, Q., Zhou, A., and Jin, Y. Rm-meda: A regularity model-based multiobjective estimation of distribution algorithm. *IEEE Transactions on Evolutionary Computation*, 12(1):41–63, 2008.
- Zhang, X., Lin, X., Xue, B., Chen, Y., and Zhang, Q. Hypervolume maximization: A geometric view of pareto set learning. In *Thirty-seventh Conference on Neural Information Processing Systems*, 2023.
- Zhao, H. and Gordon, G. J. Inherent tradeoffs in learning fair representations. *The Journal of Machine Learning Research*, 23(1):2527–2552, 2022.
- Zuluaga, M., Krause, A., and Püschel, M. ϵ -pal: an active learning approach to the multi-objective optimization problem. *The Journal of Machine Learning Research*, 17(1):3619–3650, 2016.

A. Methodology

A.1. MOO theories

As a preliminary, we introduce some basic MOO properties which used in the main paper. The definition of an aggregation function is adopted and modified from (Miettinen, 1999, Chapter 2.6), where it was originally under the name of value functions.

Definition A.1 (Aggregation function). An aggregation function $g(\cdot) : \mathbb{R}^m \mapsto \mathbb{R}$. $g(\cdot)$ is a decreasing function, i.e., $g(x) < g(x')$, if $x_i < x'_i, \forall i \in [m]$.

One example of aggregation function is the modified Tchebycheff function (Equation (2)) studied in the main paper. We have the following Lemmas (adopted and modified from (Miettinen, 1999, Theorem 2.6.2)) for an aggregation function,

Lemma A.2. Let \mathbf{y}^* be one of the optimal solution of $g(\cdot, \boldsymbol{\lambda})$, then \mathbf{y}^* is (weakly) Pareto optimal.

Lemma A.3. Let \mathbf{y}^* be the only optimal solution of $g(\cdot, \boldsymbol{\lambda})$, then \mathbf{y}^* is Pareto optimal.

Definition A.4 (Weakly Pareto Optimal Solution). $\mathbf{x}^{(a)}$ is a weakly Pareto solution if there is no other solution $\mathbf{x}^{(b)} \in \mathcal{X}$ such that $\mathbf{f}(\mathbf{x}^{(b)}) \prec \mathbf{f}(\mathbf{x}^{(a)})$, where $\mathbf{f}(\mathbf{x}^{(b)}) \prec \mathbf{f}(\mathbf{x}^{(a)})$ means $f_i(\mathbf{x}^{(b)}) < f_i(\mathbf{x}^{(a)})$ for all $i \in [m]$.

Corollary A.5. According to Lemma A.2 and A.3, for a given $\boldsymbol{\lambda}$, if there does not exist weakly Pareto solutions, the optimal solution of $g(\cdot, \boldsymbol{\lambda})$ is unique and is a Pareto solution.

B. Missing proofs

Proof. The proof has two steps. The first step is show under Assumption 4.1, \mathbf{h} is injective. We leave it as Lemma B.1.

Lemma B.1 (Injection). We assert that $\mathbf{h}(\boldsymbol{\lambda}) = \mathbf{y} = k \cdot \boldsymbol{\lambda} + \mathbf{z}$ for each $\boldsymbol{\lambda}$, where $k \cdot \boldsymbol{\lambda} + \mathbf{z}$ represents a Pareto optimal solution. This means that for a given $\boldsymbol{\lambda}$, the corresponding \mathbf{y} is unique. Suppose there exists another $\mathbf{y}' = k' \cdot \boldsymbol{\lambda}' + \mathbf{z}$ such that $\mathbf{h}(\boldsymbol{\lambda}) = \mathbf{y}'$. If $\boldsymbol{\lambda}'$ differs from $\boldsymbol{\lambda}$, then by the definition of Pareto optimality, for at least one index j , we have $\frac{y'_j - z_j}{\lambda'_j} > \frac{y_j - z_j}{\lambda_j}$. Thus, \mathbf{y}' cannot be an optimal solution if $\boldsymbol{\lambda}' \neq \boldsymbol{\lambda}$, ensuring the injectivity of function $\mathbf{h}(\boldsymbol{\lambda})$.

With the previous lemma, Consider the function $\rho(\mathbf{x}^*) = \frac{f_i(\mathbf{x}^*) - z_i}{\lambda_i}, \forall i \in [m]$, where \mathbf{x}^* denotes the optimal solution of the modified Tchebycheff function, defined as $\mathbf{x}^* = \arg \min_{\mathbf{x} \in \mathcal{X}} \max_{i \in [m]} \left\{ \frac{f_i(\mathbf{x}) - z_i}{\lambda_i} \right\}$. Given the strict convexity of the functions f_i , the expression $\max_{i \in [m]} \frac{f_i(\mathbf{x}) - z_i}{\lambda_i}$ is also strictly convex, ensuring the uniqueness of the optimal solution \mathbf{x}^* . The value of $\boldsymbol{\lambda}$ can be derived from the equation $\boldsymbol{\lambda} = \frac{\mathbf{f}(\mathbf{x}^*) - \mathbf{z}}{\rho(\mathbf{x}^*)}$. Under the condition of Lemma B.1, $\rho(\mathbf{x}^*)$ has an analytical expression, and as a result $\boldsymbol{\lambda}(\mathbf{x}^*)$ can be expressed as:

$$\boldsymbol{\lambda}(\mathbf{x}^*) = \frac{\mathbf{f}(\mathbf{x}^*) - \mathbf{z}}{\sum_{i \in [m]} (f_i(\mathbf{x}^*) - z_i)} \quad (10)$$

This equation implies that $\boldsymbol{\lambda}$ is differentiable from \mathbf{x}^* . Therefore, the inverse function of Equation 10 exists. Since $\boldsymbol{\lambda}(\mathbf{x}^*)$, by the inverse function theorem, $\mathbf{x}^*(\boldsymbol{\lambda})$ is differentiable, making the composed function $\mathbf{h}(\boldsymbol{\lambda}) = \mathbf{f} \circ \mathbf{x}^*(\boldsymbol{\lambda})$ differentiable. The application of Lemma B.1 and uniqueness condition confirms that $\mathbf{h}(\boldsymbol{\lambda})$ is a bijection. Combined with its differentiability, this confirms that $\mathbf{h}(\boldsymbol{\lambda})$ is indeed a diffeomorphism². \square

B.1. Set Geometry

In this section, we provide several useful definitions for set geometry. These definitions main serve for two purpose: (1) to give the rigid definition of δ -dominance and (2) to prove the generalization bound of a PFL model.

In Definitions B.2 and B.3, we introduce the δ -packing and δ -covering numbers of a set \mathbf{Y} , which are the maximal number of $\delta/2$ -balls and minimal number of δ -balls one needs, to pack in and cover \mathbf{Y} , respectively. They measure the metric entropies of \mathbf{Y} ; See e.g., Vershynin (2018).

²In a recent study by Roy et al. (2023), it was shown that for a smooth linear scalarization function, the Pareto objectives are diffeomorphic to the weight simplex. Our result is a stronger result, as we give the same results for a non-smooth modified Tchebycheff function

Definition B.4 defines the diameter of \mathbf{Y} , which measures the supremum of the distances between pairs of points in \mathbf{Y} . Definition B.5 gives a partition of \mathbf{Y} , given some point set \mathcal{S} in \mathbf{Y} . Briefly, any point in \mathbf{Y} will be partitioned to the Voronoi cell that has the minimal distance to it. Intuitively, if points in \mathcal{S} are approximately evenly distributed, then they will induce Voronoi cells that have similar volumes to each other.

Finally, Hausdorff measure in Definition B.6 introduces an adaptive and accurate way to measure the volumes of different sets in a multidimensional Euclidean space. For example, a curve has a trivial zero Borel measure in \mathbb{R}^2 , yet the 1-dimensional Hausdorff measure is non-trivial and could measure its length. Likewise, for a spherical shell in \mathbb{R}^3 which has zero Borel measure, the corresponding 2-dimensional Hausdorff measures its surface area.

Definition B.2 (δ -packing, δ -packing number). A δ -packing of a set \mathbf{Y} is a collection of element $\{\mathbf{y}^{(1)}, \dots, \mathbf{y}^{(N)}\}$ such that, $\rho(\mathbf{y}^{(j)}, \mathbf{y}^{(k)}) > \delta$ for all $j \neq k$. The δ -packing number $N_{\text{pack}}(\delta, \mathbf{Y})$ is the largest cardinality among all δ -packing. Here δ is called the packing distance.

Definition B.3 (δ -covering, δ -covering number). A δ -covering of a set \mathbf{Y} with respect to a metric ρ is a set $\{\boldsymbol{\theta}^{(1)}, \dots, \boldsymbol{\theta}^{(N)}\} \subset \mathbf{Y}$ such that for each $\boldsymbol{\theta} \in \mathbf{Y}$, there exists some $i \in [N]$ such that $\rho(\boldsymbol{\theta}, \boldsymbol{\theta}^{(i)}) \leq \delta$. The δ -covering number $N_{\text{cover}}(\delta, \mathbf{Y})$ is the minimal cardinality among all δ -coverings.

Definition B.4 (Set diameter). The *diameter* of any subset $\mathbf{Y} \subseteq \mathbb{R}^m$ is defined by

$$\text{diam}(\mathbf{Y}) = \max\{\rho(\mathbf{y}^{(1)}, \mathbf{y}^{(2)}) \mid \mathbf{y}^{(1)}, \mathbf{y}^{(2)} \in \mathbf{Y}\}. \quad (11)$$

Definition B.5 (Voronoi cells (Okabe et al., 2009)). The Voronoi cells $\{\mathcal{B}_1, \dots, \mathcal{B}_N\}$ of a finite set $\mathcal{S} \subseteq \mathbf{Y}$, where $\mathcal{S} = \{\mathbf{y}^{(1)}, \dots, \mathbf{y}^{(N)}\}$, is defined by,

$$\mathcal{B}_i = \left\{ \mathbf{y} \mid \min_{\mathbf{y} \in \mathbf{Y}} \rho(\mathbf{y}, \mathbf{y}^{(i)}) \right\}, \quad \forall i \in [N]. \quad (12)$$

Definition B.6 (Hausdorff measure). Consider the metric space (\mathbb{R}^m, ρ) where $\rho(\cdot, \star)$ is the Euclidean distance. The d -dimensional *Hausdorff measure* of any Borel set $\mathbf{Y} \subseteq \mathbb{R}^m$ is

$$\mathcal{H}_d(\mathbf{Y}) = \lim_{\delta \rightarrow 0} \inf_{\substack{\mathcal{Y} \subseteq \cup_{i=1}^{\infty} \mathcal{U}_i \\ \text{diam}(\mathcal{U}_i) < \delta}} \left[\sum_{i=1}^{\infty} \{\text{diam}(\mathcal{U}_i)\}^d \right], \quad d \in (0, m).$$

We use Hausdorff measure to further define the Hausdorff dimension of a set. We first introduce the following Theorem B.7 (Folland, 1999), which guarantees that, for any \mathbf{Y} , there exists at most one $d^\dagger \in \mathbb{R}$ which makes the d^\dagger -dimensional Hausdorff measure of \mathbf{Y} both non-zero and finite. We call this d^\dagger the Hausdorff dimension of \mathbf{Y} .

Theorem B.7. For any Borel set $\mathbf{Y} \subseteq \mathbb{R}^m$, suppose that for some d^\dagger , $0 < \mathcal{H}_{d^\dagger}(\mathbf{Y}) < \infty$. Then we have $\mathcal{H}_{d'}(\mathbf{Y}) = 0$ for any $d' < d^\dagger$ and $\mathcal{H}_{d'}(\mathbf{Y}) = \infty$ for any $d' > d^\dagger$.

Definition B.8 (Hausdorff dimension). We say the *Hausdorff dimension* of \mathbf{Y} is d^\dagger if and only if, $0 < \mathcal{H}_{d^\dagger}(\mathbf{Y}) < \infty$.

B.2. Notation Table

For clarity, we present a notation explanation in Table 4.

B.3. Algorithm

The total algorithms run as Algorithm 1 and 2. The proposed algorithm mainly adopt the MOEA/D framework. For simplicity, we use the Simulated Binary Crossover (SBX) (Deb et al., 1995) and poly-nominal mutation operators (Deb & Deb, 2014). It is possible to use more advanced MOEA/D framework, e.g., MOEA/D with differential evolution (Tan et al., 2012), which is left as future works.

As summarized by Algorithm 1, the proposed approach dynamically adjusts the weight angles on the estimated PF learned by the current objectives. The updated weights are then set as the new weights for the MOEA/D algorithm.

Table 4. Notations used in this paper.

Notation	Meaning	Dimension
N	Number of solutions.	-
n	Dimension of a solution.	-
m	Number of objectives.	-
\mathbf{x}	An MOO solution.	n
\mathcal{X}	The decision space. $\mathbf{x} \in \mathcal{X}$	\mathbb{R}^n
$\mathbf{y}, \mathbf{f}(\mathbf{x})$	The objective vector of a solution \mathbf{x} .	m
\mathcal{Y}	The objective space.	\mathbb{R}^m
\mathcal{S}	A set of objectives, $\mathcal{S} = \{\mathbf{y}^{(1)}, \dots, \mathbf{y}^{(N)}\}$.	m
\mathcal{T}	The Pareto front.	\mathbb{R}^m
δ	The minimal separation distance of a set belong to \mathcal{T} (c.f. Equation (6)).	
δ_v	The maximal diameter of all Voronoi cells. (c.f. Equation (20)).	
$\boldsymbol{\lambda}$	The weight vector.	m
$\boldsymbol{\theta}(\boldsymbol{\lambda}), \boldsymbol{\theta}$	The angular parameterization of vector $\boldsymbol{\lambda}$ (c.f. Equation (13)).	$m - 1$
$g^{\text{alg}}(\cdot \boldsymbol{\lambda})$	The multiobjective aggregation function.	$\mathbb{R}^m \mapsto \mathbb{R}$
$\mathbf{h}(\boldsymbol{\lambda})$	The function maps a weight to a Pareto solution. $\mathbf{h}(\boldsymbol{\lambda}) : \boldsymbol{\Omega} \mapsto \mathbb{R}^m$.	
$\mathbf{h}_\phi(\cdot)$	The PFL model. $\mathbf{h}_\phi(\cdot) : [0, \frac{\pi}{2}]^{m-1} \mapsto \mathbb{R}^m$	
$\mathcal{H}_d(\cdot)$	Hausdorff dimension function.	

Algorithm 1 Training of PFL and weight adjustment.

Input: weight angle set Θ_N and objective set \mathcal{S} from MOEA/D.

Training the PFL model.

for $i=1:N_{\text{pfl}}$ **do**

$\phi \leftarrow \hat{\phi} - \tilde{\eta} \nabla_{\phi} l_{\text{pfl}}$.

end

Solving the maximal separation problem at the estimated PF (Problem (7)) by gradient ascent.

for $i=1:N_{\text{opt}}$ **do**

$\Theta_N \leftarrow \text{Proj}(\Theta_N + \eta \nabla_{\Theta_N} \hat{\delta}_{\hat{\tau}})$.

end

Output: The updated weight angles $\{\boldsymbol{\theta}^{(1)}, \dots, \boldsymbol{\theta}^{(N)}\}$.

Algorithm 2 MOEA/D with uniform adaptive weight adjustment (UMOEAD/D).

Input: Initial N weight $\lambda_N : \lambda_N = \{\lambda^{(1)}, \dots, \lambda^{(N)}\}$ by (Das & Dennis, 1998), the initial solution set $\mathcal{X}_N : \mathcal{X}_N = \{\mathbf{x}^{(1)}, \dots, \mathbf{x}^{(N)}\}$, the MOO objective function $f(\cdot)$.

```

for  $k=1:K$  do
  for  $i=1:N_{inner}$  do
    # Step 1. Evolutionary algorithm.
    for  $j=1:N$  do
      # Generate a crossover solution from neighbourhoods of  $\mathbf{x}^{(j)}$  using SBX operator.
       $\mathbf{x}^{(j)} \leftarrow \text{SBX}(\mathbf{x}^{(j_1)}, \mathbf{x}^{(j_2)})$ , where  $\mathbf{x}^{(j_1)}, \mathbf{x}^{(j_2)}$  are selected randomly from the neighborhood set of  $\mathbf{x}^{(j)}$ .
      # Mutation the solution by the polynomial mutation operator.
       $\mathbf{x}^{(j)} \leftarrow \text{Mutate}(\mathbf{x}^{(j)})$ .
    end
    # Update the solution each sub-problems by elites.
    for  $j=1:N$  do
       $\mathbf{x}^{(j)} \leftarrow \arg \min_{i \in B(j) \cup \{x^{(j)}\}} g^{\text{miche}}(f(\mathbf{x}^i), \lambda^{(j)})$ . #  $B(j)$  is the neighborhood index set (Zhang & Li, 2007) of solution  $\mathbf{x}^{(j)}$ .
    end
  end
  # Step 2. weight adjustment.
  Calculate the weight angle set  $\Theta_N$  from weights by Equation (13).
   $\mathcal{S} = f \circ \mathcal{X}_N$ .
   $\Theta_N \leftarrow \text{Algorithm1}(\Theta_N, \mathcal{S})$ .
  Update the weight vector  $\lambda^{(1)}, \dots, \lambda^{(N)}$  by Equation (13).
end

```

We briefly analyze the running complexity of the proposed method. The main complexity is inherited from MOEA/D (Zhang & Li, 2007). The addition of the PFL model training and the uniformity optimization introduces two additional parts.

Training the PFL model is a standard supervised learning problem, hence the complexity is proportional to the number of objectives m and sample numbers N . The overall complexity is $\mathcal{O}(mN \cdot N_{\text{pfl}})$.

The uniformity optimization involves calculating the lower (or upper) triangular matrix of an adjacency matrix, which has a complexity of $\mathcal{O}(m \cdot \frac{N(N-1)}{2}) = \mathcal{O}(mN^2)$. Therefore, the total complexity of the optimization process is $\mathcal{O}(mN_{\text{opt}} \cdot \frac{mN(N-1)}{2}) = \mathcal{O}(mN^2 \cdot N_{\text{opt}})$.

Practically, training time of the PFL and weight adjustment is less than 1s, which is neglectable compared with MOEAs. The calculation of the adjacency matrix and the MOEA/D algorithm can be executed in parallel, which can further improve the efficiency of the overall running time.

(The relation between weight angle $\theta(\lambda)$ and weight λ .) Given $\theta(\lambda) \in [0, \frac{\pi}{2}]^{m-1}$ as a parameter representation of $\lambda \in \Delta_{m-1}$, the weight angle and the corresponding weight vector can be converted using the following equations:

$$\begin{cases} \sqrt{\lambda_1} = \cos(\theta_1) \\ \sqrt{\lambda_2} = \sin(\theta_1) \cos(\theta_2) \\ \sqrt{\lambda_3} = \sin(\theta_1) \sin(\theta_2) \cos(\theta_3) \\ \vdots \\ \sqrt{\lambda_m} = \sin(\theta_1) \sin(\theta_2) \dots \sin(\theta_{m-1}). \end{cases} \quad (13)$$

For a given weight vector λ , computing the weight angle can be achieved by solving Equation (13). Similarly, θ can be

solved from λ by the following equation,

$$\left\{ \begin{array}{l} \theta_1 = \arg \cos(\sqrt{\lambda_1}) \\ \theta_2 = \arg \cos\left(\frac{\sqrt{\lambda_2}}{\sin \theta_1}\right) \\ \theta_3 = \arg \cos\left(\frac{\sqrt{\lambda_3}}{\sin \theta_1 \sin \theta_2}\right) \\ \vdots \\ \theta_{m-1} = \arg \cos\left(\frac{\sqrt{\lambda_{m-1}}}{\sin \theta_1 \sin \theta_2 \dots \sin \theta_{m-1}}\right) \end{array} \right. \quad (14)$$

C. Experiments Details

C.1. Comparison Methods

We give a detailed elaboration of the comparison methods used in the experiments as follows. The code for the proposed method will be made publicly available after publication.

1. The vanilla **MOEA/D** method (Zhang & Li, 2007) employs diverse distributed weight vectors to explore a diverse Pareto solution set. However, the uniformity observed in the weight space may not lead to uniformity in the objective space, resulting in a coarse level of solution diversity sought by MOEA/D.
2. The MOEA/D with adaptive weight adjustment (**MOEA/D-AWA**) (Qi et al., 2014; de Farias et al., 2018). MOEA/D-AWA is an improvement over the vanilla MOEA/D, which aims to improve the replaces the most crowded solution with the most sparse solution. A detailed comparison of MOEA/D-AWA and the proposed method can be found in Appendix C.4.

Since the source code for their implementation was not publicly available, we implemented it by ourselves. In the original implementation of MOEA/D-AWA, they maintain an external population (EP). However, as the modern MOEA frameworks (e.g., pymoo, platemo) are no longer dependent on EP, we employ a neural network surrogate model to predict the most sparse solution (Qi et al., 2014).

3. The Pareto adaptive weight (**PaLam**) method (Siwei et al., 2011) approximates the PF using a simple math mode $y_1^p + y_2^p = 1$ and generates uniform Pareto objectives by utilizing the hypervolume indicator (Guerreiro et al., 2020). Since real-world problems often exhibit complex PFs, to ensure fairness, we employ a neural model for training to predict the true PF instead of relying on a simple mathematical model. We use the code in https://github.com/timodeist/multi_objective_learning to develop a new gradient-based algorithm for pa λ to achieve fast optimization for the HV indicator predicted by neural networks. Our improved version of the vanilla pa λ significantly outperforms its original implementation.
4. The **SMS-EMOA** (Beume et al., 2007) method, which uses the hypervolume indicator as the guidance for the multiobjective evolutionary optimizations. The code for SMS-EMOA directly follows the pymoo library.
5. The **MOEA/D-GP** (Wu et al., 2017) method. This method employs Gaussian process (GP) modeling to capture the shape of the PF and utilizes the objective function $\sum_{1 \leq i \neq j \leq N} \frac{1}{d_{ij}}$, where d_{ij} represents the distance from objective $y^{(i)}$ to $y^{(j)}$, to promote the generation of uniformly distributed Pareto objectives. In comparison to MOEA/D-GP, our method offers two significant advantages. Firstly, our method employs more accurate neural models to characterize the preference-to-objective mapping function. This allows for a more precise representation of the relationship between preferences and objectives, leading to enhanced modeling capabilities. Additionally, the adapted uniform indicator in our method is optimized more efficiently. Instead of calculating the gradients of all objectives, we only need to compute the gradients of two objectives. This optimization technique improves computational efficiency without sacrificing the quality of the results. Furthermore, our method provides superior theoretical guarantees than MOEA/D-GP.
6. The **MOEA/D-L** (Dong et al., 2020) method. This method suggests utilizing linear chains as a means to model the shape of the PF. However, due to their limited representational capacity, linear models may not be well-suited for

capturing the complexities of complex and high-dimensional PFs. Consequently, the performance of MOEA/D-L falls short compared to our proposed UMOEA/D method.

C.2. Metrics

In order to measure the performance of our proposed method, we employ the following metrics to measure uniformity and the solution quality. The up-arrow (\uparrow)/down-arrow (\downarrow) signifies that a higher/lower value of this indicator is preferable.

1. The `hypervolume` (\uparrow) (HV) indicator (Guerreiro et al., 2020), which serves as a measure of the convergence (the distance to the PF) and only a *coarse* measure of the sparsity/uniformity level of a solution set.
2. The `sparsity` (\downarrow) indicator (Xu et al., 2020), which measures the sum of distance of a set of solutions in the non-dominated sorting order (Deb et al., 2002a).
3. The `spacing` (\downarrow) indicator (Schott, 1995), which measures the uniformity of a set of solutions. It is quantified as the standard deviation of the distance set $\{d_1, \dots, d_N\}$.

$$\text{spacing}(\mathcal{S}) = \text{std}(d_1, \dots, d_N), \quad (15)$$

where $d_i = \min_{j \in [m], j \neq i} \rho(\mathbf{y}^{(i)}, \mathbf{y}^{(j)})$, serving as the minimal distance from solution $\mathbf{y}^{(i)}$ to the rest of objectives.

4. The δ (\uparrow) and $\tilde{\delta}$ (\uparrow) indicators represent the (soft) minimal distances among different solutions within a solution set.

$$\tilde{\delta} = -\frac{1}{K} \log \sum_{1 \leq i \neq j \leq N} \exp(-K \cdot \rho(\mathbf{y}^{(i)}, \mathbf{y}^{(j)})). \quad (16)$$

A large $\delta/\tilde{\delta}$ indicator means that, any different solution pairs are far away from each other. Noted that, it is possible that $\tilde{\delta} < 0$. K is a positive constant.

C.3. Results on all problems

In this subsection, we visualize the results on representative problems through Figure 6 to 11. Those figures depict the outcomes of MOEA/D, SMS-EMOA, MOEA/D-GP, MOEA/D-L, PaLam, MOEA/D-AWA, and the proposed UMOEA/D. Numerical results are shown in Table 5 and Table 6. (Soft) Optimal distances between minimal Pareto objectives are marked in bold. Except for RE42, our method achieve the optimal pairwise distances among all problems. For RE42, SMS-EMOA has the optimal distance value, however SMS-EMOA has not converged on this paper.

As we have mentioned in the main paper, the hypervolume indicator is only a coarse indicator to measure the uniformity level. The introduction of it is mainly to determine whether the algorithm has converged or not. So we do not mark the highest hypervolume indicator in bold in Appendix.

We summarize the key experimental findings as follows.

(Neighbour distances are equal in two-objective problems). For the standard ZDT1 and ZDT2 problems, which have a PF ranging from zero to one, the Pareto objectives optimized by MOEA/D are not uniformly distributed. However, our method ensures that the distance between adjacent solutions is equal, indicating a more uniform distribution. For MOEA/D, when considering a convex-shaped PF like ZDT1, solutions tend to be denser in the middle. Conversely, for a concave-shaped PF like ZDT2, solutions are denser towards the margins. However, the proposed method’s Pareto objective distribution remains unaffected by the shape of the true PF.

(The proposed method is robust to objectives with different scales). When function ranges differ in scale (see Figure 7), the uniformity of pure MOEA/D worsens. In this scenario, achieving weight uniformity does not guarantee objective uniformity. Solutions become even sparser in the upper-left region of the objective space. In contrast, the proposed method consistently generates uniform Pareto objectives. Hypervolume-based methods remain unaffected when function objectives have different scales. However, objectives produced by hypervolume-based methods are not strictly uniform, and hypervolume-based methods are typically slower.

(HV is not a accurate uniformity indicator). The hypervolume indicator only provides an approximate measure of solution diversity. Table ?? illustrates that similar hypervolume indicators can correspond to significantly different solution distributions. In the case of hypervolume-based methods (PaLam or SMS-EMOA), the largest hypervolume indicator does not necessarily lead to the most uniform objectives for most problems.

(Weight uniformity induces solution uniformity in DTLZ1). As mentioned in examples in the main paper, the PF of DTLZ1 can be represented as an affine transformation of the 2-simplex Δ_2 , since $h(\mathbf{x}) = \frac{1}{2}\mathbf{x}$. For problems considered in this paper, DTLZ1 is the only scenario where uniform weights result in uniformly distributed Pareto objectives. Hence, MOEA/D with uniform weights performs exceptionally well on the DTLZ1 task. The maximal manifold separation indicator, δ , outperforms all other methods, and the proposed method achieves a value of $\delta = 0.099$, which is very close to that of MOEA/D and significantly outperforms other methods.

(Results on the difficult RE37/RE41/RE42 problem). Finally, we present the results for the challenging three-objective real-world problem RE37/RE41/RE42. One of the difficulties of this problem is the presence of many weights within the weight simplex Δ_2 that do not intersect with the PF. The pure MOEA/D algorithm produces numerous duplicate solutions when weights do not intersect with the PF, resulting in wasted resources and poor solution diversity. The hypervolume-based method SMS-EMOA exhibits an interesting phenomenon: it mainly focuses on the marginal region of the PF, which may not always meet user demands. In contrast, the proposed method is the only method that generates uniform objectives that cover the entire PF.

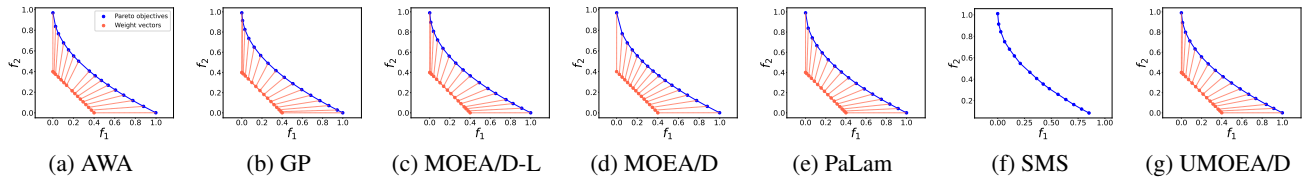


Figure 6. Results on ZDT1.

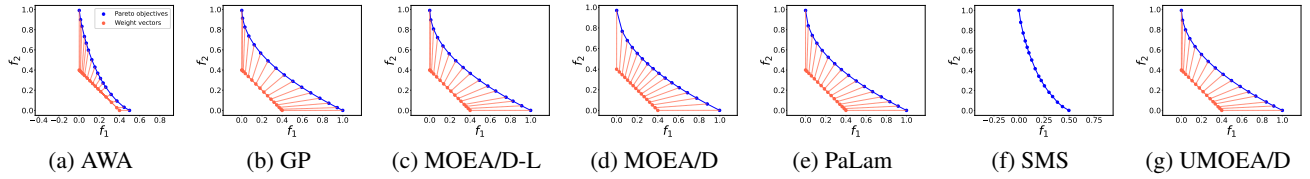


Figure 7. Results on RE21.

For three-objective problems, since DTLZ 2-4 share the same PF. We take DTLZ2 as a representative, as shown in Figure 8. We also show the projection on the difficult four-objective RE41 and RE42 problem as shown in Figure 10 and Figure 11.

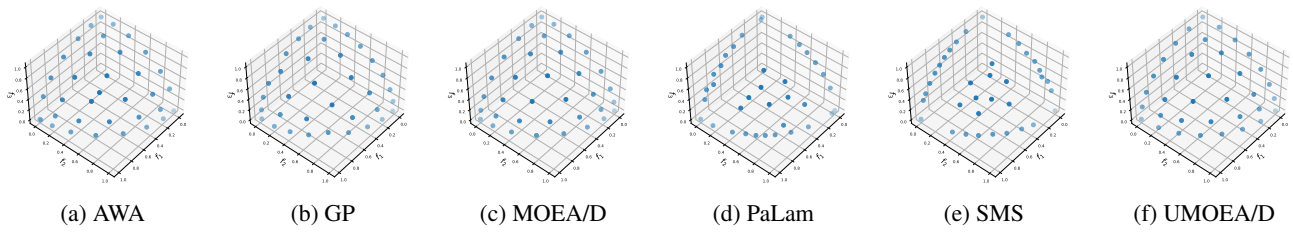


Figure 8. Results on DTLZ2.

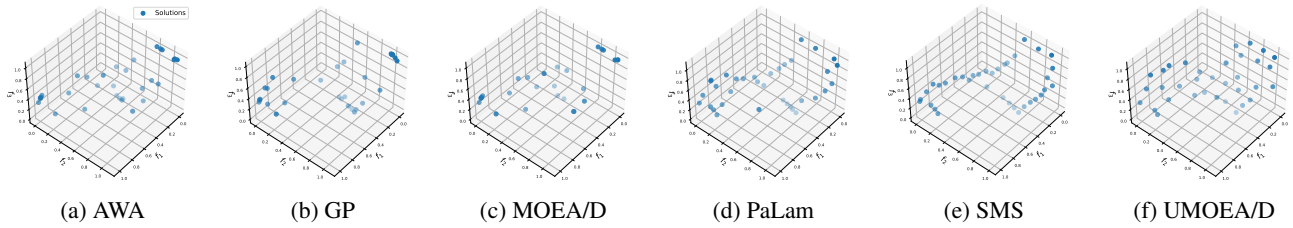


Figure 9. Results on RE37.

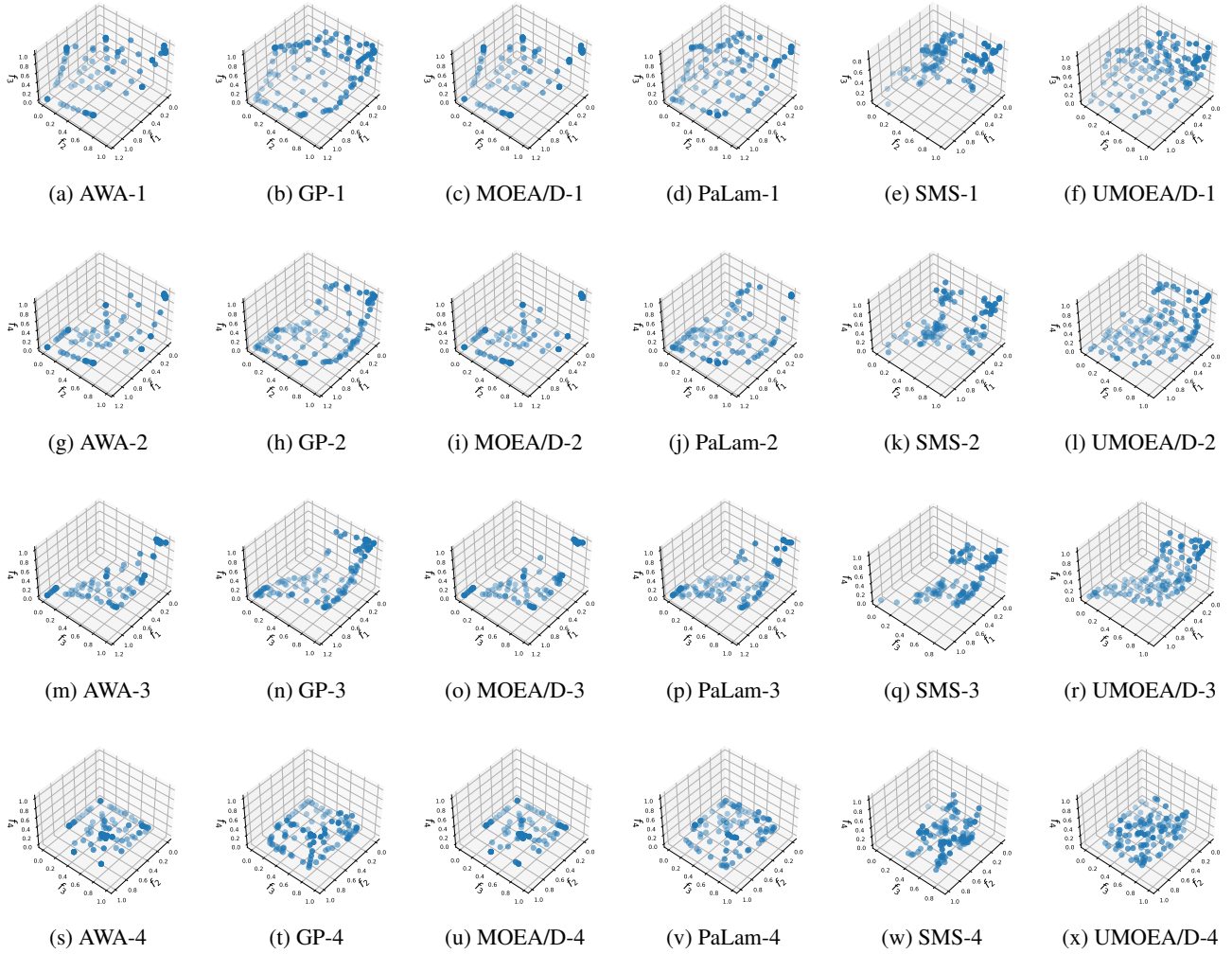


Figure 10. Results on RE41.

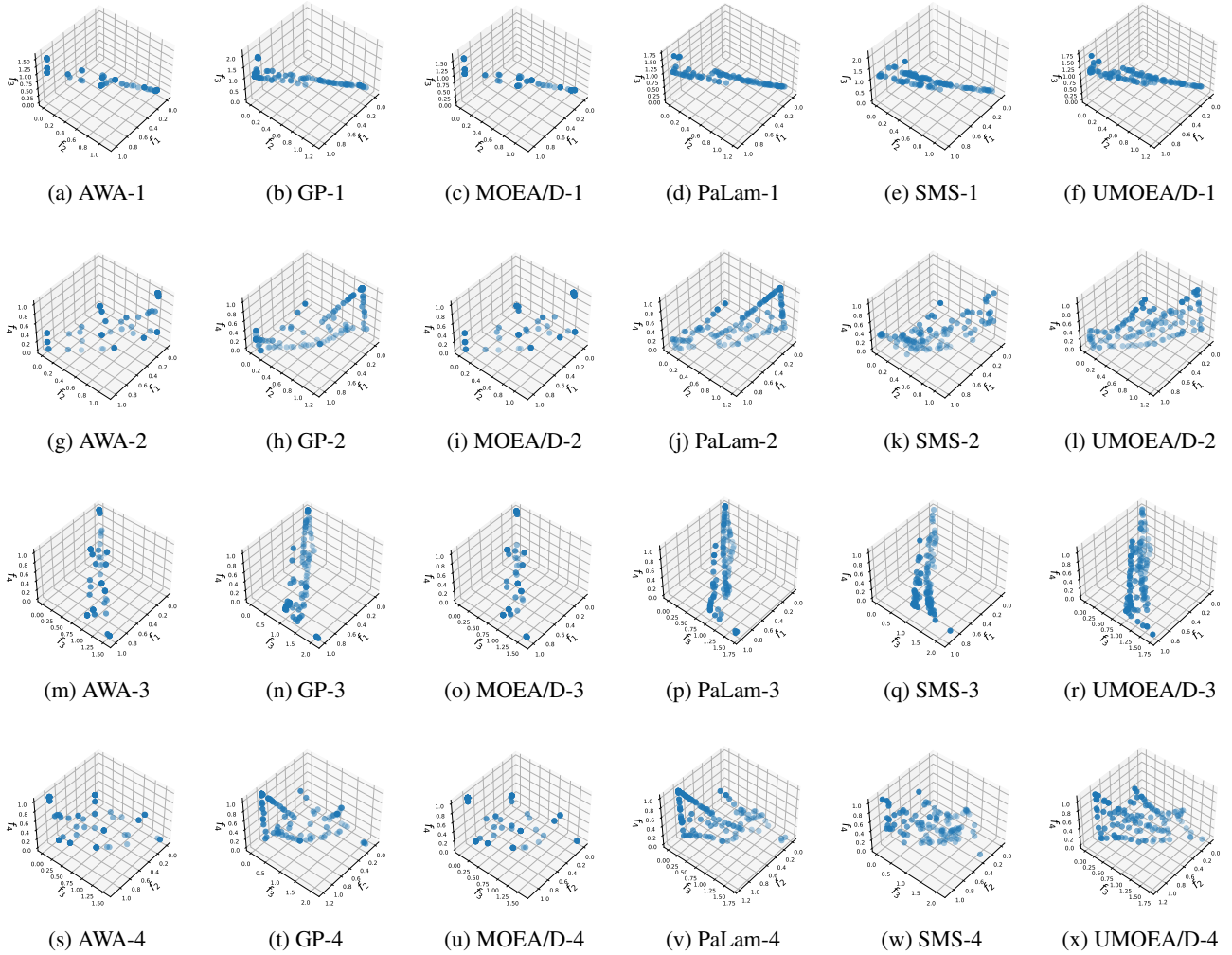


Figure 11. Results on RE42.

Table 5. Results on two-objective problems averaged on five random seeds.

Method	HV	Spacing	Sparsity	δ	$\tilde{\delta}_T$
ZDT1					
SMS-EMOA	1.2620	0.0143	0.0064	0.0489	-0.1101
MOEA/D-AWA	1.2609	0.0308	0.0073	0.0000	-0.1195
MOEA/D-GP	1.2626	0.0175	0.0061	0.0331	-0.1059
MOEAD-L	1.2628	0.0090	0.0060	0.0479	-0.1052
MOEA/D	1.2589	0.0553	0.0090	0.0432	-0.1304
PaLam	1.2634	0.0122	0.0061	0.0621	-0.1070
UMOEAD/D	1.2634	0.0026	0.0059	0.0720	-0.1046
ZDT2					
SMS-EMOA	0.4077	0.0153	0.0020	0.0144	-0.1780
MOEA/D-AWA	0.7418	0.0155	0.0099	0.0744	-0.0813
MOEA/D-GP	0.7421	0.0124	0.0098	0.0741	-0.0799
MOEAD-L	0.7423	0.0086	0.0100	0.0797	-0.0810
MOEA/D	0.7418	0.0160	0.0099	0.0702	-0.0813
PaLam	0.7435	0.0256	0.0106	0.0388	-0.0867
UMOEAD/D	0.7429	0.0082	0.0099	0.0814	-0.0800
ZDT4					
SMS-EMOA	0.0785	1.1220	8.2860	0.0212	-0.0883
MOEA/D-AWA	1.0708	0.0259	0.0109	0.0580	-0.0832
MOEA/D-GP	1.0731	0.0142	0.0097	0.0646	-0.0805
MOEAD-L	1.0731	0.0042	0.0097	0.0865	-0.0797
MOEA/D	1.0718	0.0349	0.0105	0.0704	-0.0927
PaLam	1.0748	0.0120	0.0098	0.0872	-0.0811
UMOEAD/D	1.0738	0.0036	0.0096	0.0879	-0.0794
ZDT6					
SMS-EMOA	0.5808	0.0382	0.0077	0.0204	-0.1296
MOEA/D-AWA	0.6867	0.0152	0.0064	0.0425	-0.1040
MOEA/D-GP	0.6873	0.0093	0.0063	0.0623	-0.1025
MOEAD-L	0.6876	0.0019	0.0063	0.0723	-0.1021
MOEA/D	0.6867	0.0125	0.0064	0.0548	-0.1040
PaLam	0.6878	0.0072	0.0063	0.0605	-0.1021
UMOEAD/D	0.6877	0.0019	0.0062	0.0730	-0.1018
RE21					
SMS-EMOA	1.2621	0.0179	0.0062	0.0519	-0.1100
MOEA/D-AWA	1.2616	0.0197	0.0065	0.0286	-0.1092
MOEA/D-GP	1.2627	0.0165	0.0061	0.0369	-0.1058
MOEAD-L	1.2631	0.0049	0.0060	0.0656	-0.1053
MOEA/D	1.2591	0.0553	0.0090	0.0432	-0.1304
PaLam	1.2637	0.0121	0.0061	0.0627	-0.1070
UMOEAD/D	1.2632	0.0044	0.0059	0.0656	-0.1048
RE22					
SMS-EMOA	1.2007	0.0167	0.0065	0.0418	-0.1062
MOEA/D-AWA	1.2005	0.0152	0.0063	0.0485	-0.1084
MOEA/D-GP	1.2006	0.0235	0.0065	0.0227	-0.1092
MOEAD-L	1.2004	0.0071	0.0062	0.0633	-0.1041
MOEA/D	1.1984	0.0317	0.0074	0.0329	-0.1242
PaLam	1.2013	0.0128	0.0063	0.0475	-0.1049
UMOEAD/D	1.2008	0.0044	0.0061	0.0663	-0.1041

Table 6. Results on three-objective and four-objective problems averaged on five random seeds.

Method	HV	Spacing	Sparsity	δ	$\hat{\delta}$
DTLZ1					
SMS-EMOA	1.6971	0.0098	0.0014	0.0619	-0.1723
MOEA/D-AWA	1.6955	0.0054	0.0030	0.0775	-0.1682
MOEA/D-GP	1.6963	0.0193	0.0012	0.0410	-0.1715
MOEA/D	1.6957	0.0002	0.0030	0.1002	-0.1696
PaLam	1.6973	0.0122	0.0012	0.0516	-0.1712
UMOEAD	1.6967	0.0007	0.0030	0.0988	-0.1694
DTLZ2					
SMS-EMOA	1.1166	0.0566	0.0103	0.0819	-0.0781
MOEA/D-AWA	1.1010	0.0475	0.0079	0.1155	-0.0266
MOEA/D-GP	1.0902	0.0432	0.0062	0.1517	-0.0258
MOEA/D	1.1000	0.0446	0.0080	0.1640	-0.0194
PaLam	1.1116	0.0555	0.0067	0.0380	-0.0652
UMOEAD	1.1041	0.0236	0.0110	0.2011	-0.0069
DTLZ3					
SMS-EMOA	1.1105	0.0524	0.0103	0.0952	-0.0727
MOEA/D-AWA	1.1012	0.0460	0.0076	0.1112	-0.0267
MOEA/D-GP	1.0850	0.0471	0.0062	0.1093	-0.0363
MOEA/D	1.0980	0.0447	0.0080	0.1636	-0.0191
PaLam	1.1108	0.0534	0.0069	0.0443	-0.0722
UMOEAD	1.1022	0.0221	0.0111	0.2171	-0.0061
DTLZ4					
SMS-EMOA	1.1168	0.0532	0.0102	0.1002	-0.0779
MOEA/D-AWA	1.1020	0.0421	0.0079	0.1392	-0.0193
MOEA/D-GP	1.0921	0.0420	0.0054	0.1604	-0.0236
MOEA/D	1.0999	0.0446	0.0080	0.1640	-0.0194
PaLam	1.1155	0.0491	0.0076	0.1067	-0.0616
UMOEAD	1.1037	0.0225	0.0110	0.2197	-0.0066
RE37					
SMS-EMOA	1.1143	0.0423	0.0052	0.0294	-0.1270
MOEA/D-AWA	1.0768	0.0797	0.0101	0.0012	-0.2055
MOEA/D-GP	1.0737	0.0715	0.0083	0.0023	-0.1723
MOEA/D	1.0519	0.0758	0.0122	0.0000	-0.2055
PaLam	1.1150	0.0712	0.0050	0.0023	-0.1473
UMOEAD	1.1114	0.0416	0.0047	0.0483	-0.0805
RE41					
SMS-EMOA	1.0976	0.0516	0.0014	0.0037	-0.2458
MOEA/D-AWA	1.1432	0.0676	0.0026	0.0000	-0.3001
MOEA/D-GP	1.1694	0.0687	0.0013	0.0001	-0.2798
MOEA/D	1.1328	0.0578	0.0034	0.0000	-0.2998
PaLam	1.2075	0.0551	0.0009	0.0019	-0.2352
UMOEAD	1.2072	0.0436	0.0008	0.0060	-0.1876
RE42					
SMS-EMOA	0.6080	0.0505	0.0018	0.0009	-0.2749
MOEA/D-AWA	0.5927	0.0463	0.0047	0.0000	-0.3455
MOEA/D-GP	0.6639	0.0512	0.0028	0.0000	-0.3058
MOEA/D	0.5872	0.0466	0.0052	0.0000	-0.3469
PaLam	0.6920	0.0440	0.0013	0.0002	-0.2735
UMOEAD	0.6922	0.0386	0.0019	<u>0.0007</u>	-0.2535

C.4. Difference of the proposed UMOEA/D and MOEA/D-AWA

The weight adjustment processes of MOEA/D-AWA (Qi et al., 2014) on two-objective ZDT1, three-objective DTLZ2/RE37 are demonstrated in Figure 12. During each update, the algorithm eliminates the most crowded objective (depicted as a red dot in Figure 12) and adds the most sparse objective (represented by a green dot). The resulting weight is indicated by a green star. The sparsity measure is determined using Equation (4) as outlined in the original publication (Qi et al., 2014). From Figure 12, it is evident that the initial objectives obtained by MOEA/D-mtche (MOEA/D with modified Tchebycheff aggregation function) are unevenly distributed on the (surrogate) PF. By contrast, MOEA/D-AWA successfully eliminates the most crowded objective in the upper-right region of the DTLZ2 problem, adding a new objective at the center of the PF.

However, the aforementioned strategy is heuristic in nature, lacking a guarantee of achieving optimal solutions during the final adjustment phase. Another difference is MOEA/D-AWA compared with the proposed method is that it only remove and add one solution for each weight adjustment, which make it less efficient compared with the proposed method.

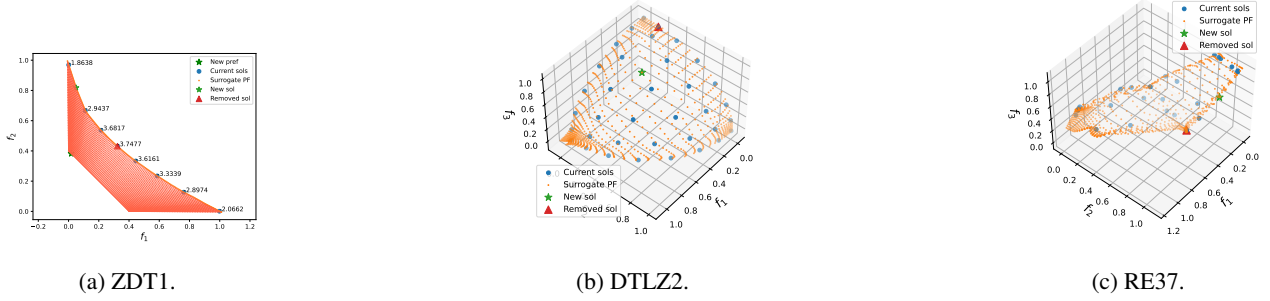


Figure 12. weight adjustment in MOEA/D-AWA.

C.5. Comparison with Gradient-based MOOs

In this section, we show that, since a large number of MOO problems have plenty of local optimal solutions, pure gradient-based methods easily fail on these problems. We take the ZDT4 problem as an example, which has the form of,

$$\begin{cases} f_1(\mathbf{x}) = x_1 \\ g(\mathbf{x}) = 1 + 10(n-1) + \sum_{i=2}^n (x_i^2 - 10 \cos(4\pi x_i)) \\ h(f_1(\mathbf{x}), g(\mathbf{x})) = 1 - \sqrt{f_1/g(\mathbf{x})} \\ f_2(\mathbf{x}) = g(\mathbf{x}) \cdot h(f_1(\mathbf{x}), g(\mathbf{x})) \\ 0 \leq x_1 \leq 1, \\ -10 \leq x_i \leq 10, \quad i = 2, \dots, n. \end{cases} \quad (17)$$

It is clear that due to the term $\sum_{i=2}^n (x_i^2 - 10 \cos(4\pi x_i))$, the objective function has plenty of locally optimas. Simply using gradient methods fails on this problems. The left figure in Figure 13 is using the simple linear aggregation function (weighted sum), where $g(\mathbf{f}(\mathbf{x}), \boldsymbol{\lambda}) = \sum_{i=1}^m \lambda_i f_i(\mathbf{x})$. And the left figure use the modified Tchebycheff aggregation function as defined by Equation (2). By directly optimizing this aggregation functions by gradient descent methods, the second objective f_2 keeps a very large value which is far from the global optimal.

The gradient of an aggregation function can be decomposed by the chain rule as: $\frac{\partial g}{\partial \mathbf{x}} = \sum_{i=1}^m \frac{\partial g}{\partial f_i} \cdot \frac{\partial f_i}{\partial \mathbf{x}}$. However, when $\|\frac{\partial f_i}{\partial \mathbf{x}}\| = 0$ for a specific index i , the gradient information for objective f_i disappears. We would also like to mention that, recently, there emerges some new gradient-based methods called ‘Specialized Multi-Task Optimizers’ (SMTOs) (Hu et al., 2023), such as MOO-SVG (Liu et al., 2021b) or EPO (Mahapatra & Rajan, 2020).

We argue that these methods may not provide significant improvements for problems like ZDT4. The primary reason is that these methods require solving the gradients $\nabla f_i(\mathbf{x})$ for each objective and manipulating them using gradient manipulation

techniques. However, if the norm of one of these gradient information, $\|\nabla f_i(\mathbf{x})\|$, equals zero, the resulting direction lacks any information to optimize the corresponding objective. Consequently, this objective remains trapped in a local optimum.

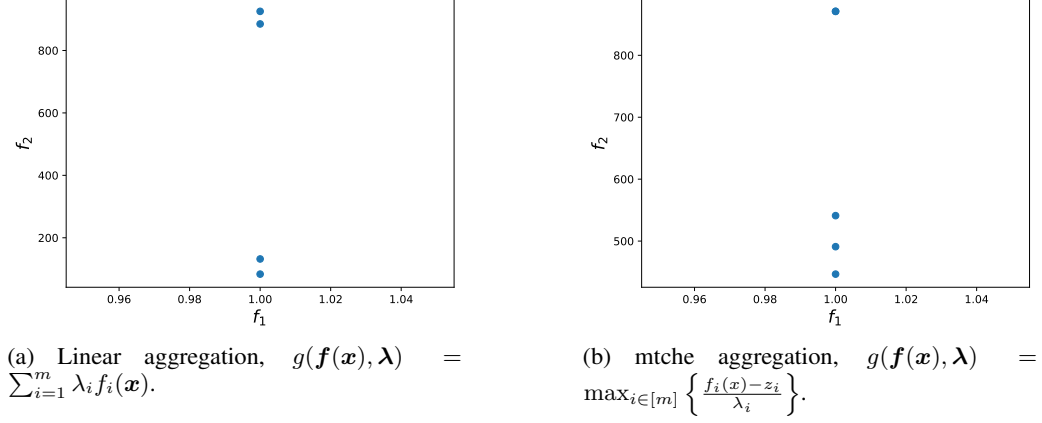


Figure 13. Results of gradient-based MOOs on ZDT4.

D. Theoretical Results

In this section, we provide theoretical results of the benefits of the uniform Pareto objectives for estimating the PF model. Section D.1 provides the preliminary tools of risk analysis which is served for Section D.2. Section D.2 proves the main Theorem 4.7 in the main paper. The other sections provide the missing proofs in Section 4.1 and 4.2.

D.1. Risk decomposition

The excess risk of the prediction model, i.e., $R(\hat{\mathbf{h}})$, can be decomposed in four parts according to Telgarsky (2021, Preface),

$$R(\hat{\mathbf{h}}) \leq \underbrace{|R(\hat{\mathbf{h}}) - \hat{R}(\hat{\mathbf{h}})|}_{\epsilon_1} + \underbrace{\hat{R}(\hat{\mathbf{h}}) - \hat{R}(\bar{\mathbf{h}})}_{\epsilon_2} + \underbrace{|\hat{R}(\bar{\mathbf{h}}) - R(\bar{\mathbf{h}})|}_{\epsilon_3} + \underbrace{R(\bar{\mathbf{h}})}_{\epsilon_4}; \quad (18)$$

Here $R(\cdot)$ denotes the true risk and $\hat{R}(\cdot)$ denotes the empirical risk with N samples, $\hat{\mathbf{h}}$ denotes the function achieved by SGD and $\bar{\mathbf{h}}$ is some low-complexity approximation of $\mathbf{h}_*(\cdot)$ in a function class \mathcal{F} of all possible neural-networks predictors.

The second term ϵ_2 is the optimization loss, which can be optimized to global optimal in a polynomial time with the network depth and input size according to Allen-Zhu et al. (2019, Th. 1). The forth term ϵ_4 is the approximation error, both of which can be small due to the universal approximation theorem with an appropriately specified \mathcal{F} ; see e.g., Telgarsky (2021, Preface).

In the next section, we give the bound of the first and third term ϵ_1 and ϵ_3 through controlling the more general generalization error. In particular, let $\tilde{\mathbf{h}} = \bar{\mathbf{h}}$ or $\hat{\mathbf{h}}$, then ϵ_1 or ϵ_3 can be expressed by the corresponding generalization error $\tilde{\epsilon} = |R(\tilde{\mathbf{h}}) - \hat{R}(\tilde{\mathbf{h}})|$.

D.2. Proof of Theorem 4.7

Proof. We firstly decompose the error $\tilde{\epsilon}$ into two parts, ϵ_1 and ϵ_2 , which can be formulated as,

$$\begin{aligned}
 \tilde{\epsilon} &= \underbrace{\int_{\mathcal{T}} \left(\left\| (\tilde{\mathbf{h}} - \mathbf{h}_*) \circ \mathbf{h}_*^{-1}(\mathbf{y}) \right\| \right)^2 d\mathbf{y}}_{R(\tilde{\mathbf{h}})} - \underbrace{\frac{1}{N} \sum_{i=1}^N \left(\left\| (\tilde{\mathbf{h}} - \mathbf{h}_*) \circ \mathbf{h}_*^{-1}(\mathbf{y}^{(i)}) \right\| \right)^2}_{\hat{R}(\tilde{\mathbf{h}})}, \\
 &\leq \underbrace{\sum_{i=1}^N \left(\int_{\mathcal{B}_i} \left(\left\| (\tilde{\mathbf{h}} - \mathbf{h}_*) \circ \mathbf{h}_*^{-1}(\mathbf{y}) \right\| \right)^2 - \left(\left\| (\tilde{\mathbf{h}} - \mathbf{h}_*) \circ \mathbf{h}_*^{-1}(\mathbf{y}^{(i)}) \right\| \right)^2 \right) d\mathbf{y}}_{\epsilon_1} \\
 &\quad + \underbrace{\sum_{i=1}^N \left(\frac{\mathcal{H}_{m-1}(\mathcal{B}_i)}{\mathcal{H}_{m-1}(\mathcal{T})} - \frac{1}{N} \right) c_i}_{\epsilon_2},
 \end{aligned} \tag{19}$$

where $\mathbf{h}_*(\cdot)$ is the true mapping function from a weight angle to Pareto solution, $\mathbf{h}_*^{-1}(\cdot)$ is the inverse function of $\mathbf{h}_*(\cdot)$ and $c_i = \left(\left\| (\tilde{\mathbf{h}} - \mathbf{h}_*) \circ \mathbf{h}_*^{-1}(\mathbf{y}^{(i)}) \right\| \right)^2 \leq A^2$. We use notation c to denote the maximal value of c_i , where $0 < c = \max_{i \in [N]} \{c_i\} \leq A^2$. In the second line in Equation (19), \mathcal{B}_i denotes the Voronoi cell of point $\mathbf{y}^{(i)}$, where $\mathcal{B}_i = \{\mathbf{y} \mid \min_{\mathbf{y} \in \mathcal{T}} \rho(\mathbf{y}, \mathbf{y}^{(i)})\}$. The distance function $\rho(\cdot, \cdot)$ remain as the ℓ_2 norm. We use δ_i to denote the diameter of set \mathcal{B}_i , where the formal definition of a diameter is provided in Equation (11). Similarly, the maximal diameter δ_v of all cells is defined as,

$$\delta_v = \max_{i \in [N]} \{\delta_i\}. \tag{20}$$

The proof primarily consists of two steps, where we separately bound ϵ_1 and ϵ_2 .

(The bound of ϵ_1) We first show that ϵ_1 can be bounded by the maximal diameter δ up to a constant.

$$\begin{aligned}
 &\sum_{i=1}^N \int_{\mathcal{B}_i} \left(\left\| (\tilde{\mathbf{h}} - \mathbf{h}_*) \circ \mathbf{h}_*^{-1}(\mathbf{y}) \right\| \right)^2 - \left(\left\| (\tilde{\mathbf{h}} - \mathbf{h}_*) \circ \mathbf{h}_*^{-1}(\mathbf{y}^{(i)}) \right\| \right)^2 d\mathbf{y} \\
 &= \sum_{i=1}^N \int_{\mathcal{B}_i} \left(\left\| (\tilde{\mathbf{h}} - \mathbf{h}_*) \circ \mathbf{h}_*^{-1}(\mathbf{y}) \right\| - \left\| (\tilde{\mathbf{h}} - \mathbf{h}_*) \circ \mathbf{h}_*^{-1}(\mathbf{y}^{(i)}) \right\| \right) \left(\left\| (\tilde{\mathbf{h}} - \mathbf{h}_*) \circ \mathbf{h}_*^{-1}(\mathbf{y}) \right\| + \left\| (\tilde{\mathbf{h}} - \mathbf{h}_*) \circ \mathbf{h}_*^{-1}(\mathbf{y}^{(i)}) \right\| \right) d\mathbf{y} \\
 &\leq \sum_{i=1}^N \int_{\mathcal{B}_i} \left(\left\| (\tilde{\mathbf{h}} - \mathbf{h}_*) \circ \mathbf{h}_*^{-1}(\mathbf{y}) - (\tilde{\mathbf{h}} - \mathbf{h}_*) \circ \mathbf{h}_*^{-1}(\mathbf{y}^{(i)}) \right\| \right) \left(\left\| (\tilde{\mathbf{h}} - \mathbf{h}_*) \circ \mathbf{h}_*^{-1}(\mathbf{y}) \right\| + \left\| (\tilde{\mathbf{h}} - \mathbf{h}_*) \circ \mathbf{h}_*^{-1}(\mathbf{y}^{(i)}) \right\| \right) d\mathbf{y} \\
 &\quad \text{(By function smoothness and upper bound)} \\
 &\leq \sum_{i=1}^N \int_{\mathcal{B}_i} 2AA'LL' \left\| \mathbf{y} - \mathbf{y}^{(i)} \right\| d\mathbf{y} \\
 &\leq \sum_{i=1}^N 2\mathcal{H}_{m-1}(\mathcal{B}_i)AA'LL'\delta_v \\
 &\leq 2\mathcal{H}_{m-1}(\mathcal{T})AA'LL'\delta_v.
 \end{aligned} \tag{21}$$

(The bound of ϵ_2) To bound ϵ_2 , we introduce several distribution functions as summarized below.

- $\mathcal{U} = \text{Unif}(\mathcal{T})$ denotes the uniform distribution over the PF \mathcal{T} .

- $\tilde{\mathbf{Y}}_N$ represents the category distribution over the set $\{\mathbf{y}^{(1)}, \dots, \mathbf{y}^{(N)}\}$, where each discrete point has a probability of $\frac{1}{N}$:
- S_N is any distribution, that satisfies the following properties. (1) $\int_{\mathcal{B}_i} p_{S_N}(\mathbf{y}) d\mathbf{y} = \frac{1}{N}$ (2) $|\partial p_{S_N}(\mathbf{y})/\partial \mathbf{y}|$ is zero at boundary and is bounded at other place, and (3) almost surely, the pointwise density of S_N is large or smaller than the corresponding pointwise density of \mathcal{U} , at each \mathcal{B}_i .

With the above distributions, we can bound ε_2 by the following derivation,

$$\begin{aligned}
 \sum_{i=1}^N \left(\frac{\mathcal{H}_{m-1}(\mathcal{B}_i)}{\mathcal{H}_{m-1}(\mathcal{T})} - \frac{1}{N} \right) c_i &\leq \sum_{i=1}^N \left| \frac{\mathcal{H}_{m-1}(\mathcal{B}_i)}{\mathcal{H}_{m-1}(\mathcal{T})} - \frac{1}{N} \right| A^2 \\
 &= CA^2 \text{TV}(\mathcal{U}, S_N) \\
 &\leq CA^2 \sqrt{\mathcal{W}_1(\mathcal{U}, S_N)} \\
 &\leq CA^2 \sqrt{\mathcal{W}_1(\mathcal{U}, \tilde{\mathbf{Y}}_N) + \mathcal{W}_1(\tilde{\mathbf{Y}}_N, S_N)} \\
 &\leq CA^2 \sqrt{\mathcal{W}_1(\mathcal{U}, \tilde{\mathbf{Y}}_N) + \delta_v}.
 \end{aligned} \tag{22}$$

Here, \mathcal{W}_1 is the Wasserstein distance function. The second line is from the definition of the total variance (TV) distance. The third line is an adaptation of (Chae & Walker, 2020, Theorem 2.1) with $\alpha = 1$ therein. As shown by (Chae & Walker, 2020, Theorem 2.1), $C > 0$ is determined by the Sobolev norms of \mathcal{U} and S_N , which can be regarded as a universal constant, since S_N has a smooth density function and \mathcal{T} is compact. The quantity $\mathcal{W}_1(\tilde{\mathbf{Y}}_N, S_N)$ can be bounded by the following expressions,

$$\begin{aligned}
 \mathcal{W}_1(\tilde{\mathbf{Y}}_N, S_N) &= \inf_{\gamma \in \Gamma} \int_{\mathcal{T} \times \mathcal{T}} |\mathbf{y} - \mathbf{y}'| \gamma(\mathbf{y}, \mathbf{y}') d\mathbf{y} d\mathbf{y}' \\
 &\leq \inf_{\gamma \in \Gamma} \sum_{i=1}^N \int_{\mathcal{T}} |\mathbf{y} - \mathbf{y}^{(i)}| \gamma(\mathbf{y}, \mathbf{y}^{(i)}) d\mathbf{y} \\
 &\leq \delta_v \inf_{\gamma \in \Gamma} \underbrace{\sum_{i=1}^N \int_{\mathcal{T}} \gamma(\mathbf{y}, \mathbf{y}^{(i)}) d\mathbf{y}}_{=1/N} = \delta_v.
 \end{aligned} \tag{23}$$

Here Γ is the set of all joint density function γ over $\mathcal{T} \times \mathcal{T}$ such that,

$$\sum_{i=1}^N \gamma(\mathbf{y}, \mathbf{y}^{(i)}) = p_{S_N}(\mathbf{y}), \quad \int_{\mathcal{T}} \gamma(\mathbf{y}, \mathbf{y}') d\mathbf{y} = \frac{1}{N} \mathbb{I}(\mathbf{y}' = y_i \text{ for some } i \in [n]),$$

which also implies that $\gamma(\mathbf{y}, \mathbf{y}') = 0$ as long as \mathbf{y}' is not in $\{\mathbf{y}^{(1)}, \dots, \mathbf{y}^{(N)}\}$. □

D.3. Proof of Proposition 4.6

The asymptotic result follows (Borodachov et al., 2007)[Theorem 2.2]. As for the non-asymptotic results, we make a proper assumption.

Assumption D.1. when the solution number $N_1 > N_2$, the packing distance solving Equation (6) is strictly decreasing, i.e., $\delta^*(N_1) < \delta^*(N_2)$.

Proof. Under this assumption, Let N_1 is the maximal packing number of $\delta^*(N_1)$. In such a case, the solution set $\mathbf{Y}_{N_1}^*$ is also a $\delta^*(N_1)$ -covering. Since when it is not a $\delta^*(N_1)$ -covering, then there exist a solution $\mathbf{y}' \in \mathcal{T}, \mathbf{y}' \neq y_i, i \in [N_1]$ such that $\rho(\mathbf{y}^{(i)}, \mathbf{y}^{(j)}) > \delta^*(N_1), i \neq j$, then $\mathcal{S}' = \{\mathbf{y}'\} \cup \mathbf{Y}_{N_1}^*$ is a $(N_1 + 1)$ packing of \mathbf{Y}_{N_1+1} , which is a contradiction. □

D.4. Special Cases for Uniform weight Yielding Uniform Pareto Objectives

The key is to show when the function $\mathbf{h}(\boldsymbol{\lambda})$ is a constant mapping with respect to the input $\boldsymbol{\lambda}$, which is a special case of affine mapping. We provide two special cases,

1. The entire weight space Ω is \mathcal{S}_1^+ or \mathcal{S}_2^+ . The objective function f is ZDT2 or DTLZ2.
2. The entire weight space Ω is Δ_2 . and the objective function f is DTLZ1.

We prove the first case as an example, and the second one can be proved similarly.

Proof. For each weight $\boldsymbol{\lambda} = (\lambda_1, \dots, \lambda_m)$, $\boldsymbol{\lambda} \in \mathcal{S}_+^{m-1}$, the corresponding solution $y = \mathbf{h}(\boldsymbol{\lambda})$ can be expressed in the form of $(k'(\boldsymbol{\lambda}) \cdot \lambda_1, \dots, k'(\boldsymbol{\lambda}) \cdot \lambda_m)$, since the function $\mathbf{h}(\boldsymbol{\lambda})$ is an “exact” mapping function. Since $(k'(\boldsymbol{\lambda}) \cdot \lambda_1, \dots, k'(\boldsymbol{\lambda}) \cdot \lambda_m)$ lies on the PF $k \cdot \mathcal{S}_+^{m-1}$, we have,

$$\begin{cases} \sum_{i=1}^m \lambda_i^2 = 1, \\ (k'(\boldsymbol{\lambda}))^2 \sum \lambda_i^2 = k^2. \end{cases} \quad (24)$$

Equation (24) directly leads that $\mathbf{h}(\boldsymbol{\lambda}) = k \cdot \boldsymbol{\lambda}$, $\forall \boldsymbol{\lambda} \in \mathcal{S}_+^{m-1}$. Thus, $\mathbf{h}(\boldsymbol{\lambda})$ maps an asymptotically uniform distribution up to a constant, which also is an asymptotically uniform distribution. \square

D.5. Proof of Theorem 4.3

Blank et al. (2020) proposed to generate uniformly distributed weight set λ_N , by solving the following optimization problem,

$$\max_{(\lambda_N \subseteq \Omega)} \min_{(i,j \in [N], i \neq j)} \rho(\boldsymbol{\lambda}^{(i)}, \boldsymbol{\lambda}^{(j)}) \quad (25)$$

where Ω is a compact connected set embedded of \mathbb{R}^m . The distance function $\rho(\cdot, \cdot)$ is adopted as the ℓ_2 norm in this paper.

To prove Theorem 4.3, we first need to introduce Lemma D.2. According to Borodachov et al. (2007), when Ω is a rectifiable set³, we have the following asymptotic uniformity of λ_N when λ_N solve Problem (25),

Lemma D.2 ((Borodachov et al., 2007)). *For any fixed Borel subset $\mathcal{B} \subseteq \Omega$, one has, when $N \rightarrow \infty$,*

$$\mathbb{P}(\tilde{\lambda}_N \in \mathcal{B}) = \frac{\text{Card}(\lambda_N \cap \mathcal{B})}{\text{Card}(\lambda_N)} \rightarrow \frac{\mathcal{H}_{m-1}(\mathcal{B})}{\mathcal{H}_{m-1}(\Omega)} = \mathbb{P}(\tilde{\lambda} \in \mathcal{B}). \quad (26)$$

We use $\text{Card}(\cdot)$ to represent the cardinality of a set. Lemma D.2 directly follows from the proof of (Borodachov et al., 2007, Theorem 2.2). Let $\tilde{\lambda}_N$ be a random variable sampled from the category distribution of the set λ_N , where each category has a probability of $\frac{1}{N}$. $\tilde{\lambda}$ is a random variable sampled from the uniform distribution on Ω , denoted as $\text{Unif}(\Omega)$. See ?? for more discussions about Hausdorff measure $\mathcal{H}_{m-1}(\cdot)$.

Lemma D.2 is equivalent to say that $\tilde{\lambda}_N \xrightarrow{d} \text{Unif}(\Omega)$. To prove Theorem 4.3, according to the continuous mapping theorem (Durrett, 2019, Theorem 3.2.10), $\tilde{\mathbf{Y}}_N = \mathbf{h} \circ \tilde{\lambda}_N \xrightarrow{d} \mathbf{h} \circ \text{Unif}(\Omega)$.

³Any compact and connected set with a finite Hausdorff dimension is a rectifiable set. As we have assumed Ω is compact and connected, then Ω is rectifiable